1976

Electroexcitation of giant resonances 6.1 MeV and 38 MeV excitation energy in [Superscript 89]Y

Shannon, James Okey

Monterey, California. Naval Postgraduate School

ELECTROEXCITATION OF GIANT RESONANCES BETWEEN 6.1 MeV AND 38 MeV EXCITATION ENERGY IN ^{89}Y

James Okey Shannon

NAVAL POSTGRADUATE SCHOOL
Monterey, California

THESIS

ELECTROEXCITATION
OF GIANT RESONANCES
BETWEEN 6.1 MeV AND 38 MeV
EXCITATION ENERGY IN ^{89}Y

by

James Okey Shannon

and

William Harold Smith

June 1976

Thesis Advisors: F.R. Buskirk
W.R. Pitthan

UNCLASSIFIED

SECURITY CLASSIFICATION OF THIS PAGE (When Data Entered)

REPORT DOCUMENTATION PAGE		READ INSTRUCTIONS BEFORE COMPLETING FORM
1. REPORT NUMBER	2. GOVT ACCESSION NO.	3. RECIPIENT'S CATALOG NUMBER
4. TITLE (and Subtitle) Electroexcitation of Giant Resonances Between 6.1 MeV and 38 MeV Excitation Energy in ^{89}Y		5. TYPE OF REPORT & PERIOD COVERED Master's Thesis; June 1976
		6. PERFORMING ORG. REPORT NUMBER
7. AUTHOR(s) James Okey Shannon William Harold Smith		8. CONTRACT OR GRANT NUMBER(s)
9. PERFORMING ORGANIZATION NAME AND ADDRESS Naval Postgraduate School Monterey, California 93940		10. PROGRAM ELEMENT, PROJECT, TASK AREA & WORK UNIT NUMBERS
11. CONTROLLING OFFICE NAME AND ADDRESS Naval Postgraduate School Monterey, California 93940		12. REPORT DATE June 1976
		13. NUMBER OF PAGES 75
14. MONITORING AGENCY NAME & ADDRESS(if different from Controlling Office)		15. SECURITY CLASS. (of this report) Unclassified
		15a. DECLASSIFICATION/DOWNGRADING SCHEDULE

16. DISTRIBUTION STATEMENT (of this Report)

Approved for public release; distribution unlimited.

17. DISTRIBUTION STATEMENT (of the abstract entered in Block 20, if different from Report)

18. SUPPLEMENTARY NOTES

19. KEY WORDS (Continue on reverse side if necessary and identify by block number)

inelastic electron scattering, giant resonances, multipole transitions, nuclear resonances, nuclear transitions, LINAC, line shape fitting, ^{89}Yttrium

20. ABSTRACT (Continue on reverse side if necessary and identify by block number)

Giant resonances in ^{89}Y were studied with inelastic scattering of 92.5 MeV incident electrons at scattering angles of 75°, 90°, 105° and 120°. In the excitation energy range of 6.1 to 38 MeV, nine transitions were observed. The

DD FORM 1 JAN 73 1473 EDITION OF 1 NOV 65 IS OBSOLETE
S/N 0102-014-6601 |
(Page 1)

UNCLASSIFIED
SECURITY CLASSIFICATION OF THIS PAGE (When Data Entered)

(20. ABSTRACT Continued)

previously reported E1 has been verified, but the broad E2 has been separated into two distinct resonances. Reduced transition probabilities and multipolarity assignments have been made. Resonances occurred at excitation energies of 6.69 (E2), 8.09 (E2), 10.01 (E2), 11.21 (E2), 12.46 (E3), 13.36 (M2 or E3), 14.86 (E2), 16.60 (E1), 27.85 (E2).

Electroexcitation of Giant Resonances Between 6.1 MeV and 38 MeV Excitation Energy in ^{89}Y

by

James Okey Shannon
Lieutenant Commander, United States Navy
B.S., United States Naval Academy, 1966

and

William Harold Smith
Lieutenant, United States Navy
B.S., United States Naval Academy, 1968

Submitted in partial fulfillment of the
requirements for the degree of

MASTER OF SCIENCE IN PHYSICS

from the

NAVAL POSTGRADUATE SCHOOL
June 1976

ABSTRACT

Giant resonances in ^{89}Y were studied with inelastic scattering of 92.5 MeV incident electrons at scattering angles of 75°, 90°, 105° and 120°. In the excitation energy range of 6.1 to 38 MeV, nine transitions were observed. The previously reported E1 has been verified, but the broad E2 has been separated into two distinct resonances. Reduced transition probabilities and multipolarity assignments have been made. Resonances occurred at excitation energies of 6.69(E2), 8.09(E2), 10.01 (E2), 11.21 (E2), 12.46 (E3), 13.63 (M2 or E3), 14.86 (E2), 16.60 (E1), 27.85 (E2).

TABLE OF CONTENTS

LIST OF TABLES

LIST OF FIGURES

ACKNOWLEDGMENTS

Successful completion and approval of this thesis can be directly attributed to our wives' understanding and encouragement, our thesis advisors' knowledge and guidance, and LINAC and computer technicians' cooperation and timely assistance. Please accept our most sincere appreciation.

I. INTRODUCTION

Inelastic electron scattering has become the major tool of investigation of giant resonance phenomena. Previous experiments with the Naval Postgraduate School Linear Accelerator have included ^{208}Pb, ^{197}Au and ^{165}Ho [Refs. (1) and (2)]. In order to make a more systematic survey of the nuclear table, it was decided to investigate medium-light nuclei. ^{89}Y was chosen because it has a closed neutron shell (N=50). Previous experience with closed shell nuclei [Refs. (3) and (4)] have shown that giant resonances in these nuclei are relatively small and can therefore be disentangled from each other. Furthermore, the neighbor nucleus ^{90}Zr is the only nucleus where a total E2 width (4.8MeV) greater than the total E1 width (4.0MeV) has been reported [Ref. (4)].

With a fixed energy incident electron beam of 92.5 MeV, data were collected at scattering angles of 75°, 90°, 105° and 120°. For each scattering angle, the number of scattered electrons was measured in the range 96 MeV to 50 MeV in order to include the elastic peak and excitation resonances from 6 to 38 MeV. Experimental inelastic cross sections were extracted for nine states and multipolarities have been assigned.

II. THEORY

A. ELECTRON SCATTERING

1. Elastic Electron Scattering

The principle of electron scattering from nuclei can be found in the derivation of scattering theory cross-sections by Rutherford and Mott. The Rutherford differential cross section for elastic scattering of charged point particles from a fixed point charge Ze is written [Ref. (5)]:

$$\left(\frac{d\sigma}{d\Omega}\right)_{RUTH} = \frac{Z^2 e^4}{16 E_i^2 \sin^4 \frac{\theta}{2}} \qquad \text{(II-1)}$$

where

θ = scattering angle

E_i = total energy of incident particle

This equation does not account for relativistic and spin effects. Mott, following Dirac's formalism for the relativistic electron, took the latter effects into account. In considering scattering from point charge centers, Mott derived the following formula for extremely relativistic Dirac particles [Ref. (6)]:

$$\left(\frac{d\sigma}{d\Omega}\right)_{MOTT} = \left[\frac{Z e^2}{2E}\right]^2 \frac{\cos^2 \frac{\theta}{2}}{\sin^4 \frac{\theta}{2}} \qquad \text{(II-2)}$$

This formula was followed by experimental confirmation using electron energies on the order of 1 MeV [Ref. (7)]. In more recent years, electron scattering has been transformed into the rapidly evolving science of nuclear structure study. Using electron beams of sufficiently high energy ($E \geq 50$ MeV) so that the electron's De Broglie wave length ($\bar{\lambda} = \bar{h}/k$) becomes equal to, or smaller than, the spatial extension of the nucleus (~ 1FERMI = 10^{-15}m), researchers began to probe the structure of the nucleus [Ref. (7)]. The angular distribution of electrons scattered is influenced by the extension and shape of the nuclear charge distribution. Therefore, experimental results which deviate from Mott cross section predictions are interpreted as arising from the finite extent of the nuclear charge density. To account for the finite size of the nucleus, a form factor representing the charge distribution of the target nucleus multiplies the Mott cross section [Ref. (8)], giving

$$\left(\frac{d\sigma}{d\Omega}\right) = \left(\frac{d\sigma}{d\Omega}\right)_{MOTT} |F(q)|^2, \qquad \text{(II-3)}$$

where

q = momentum transfer, and

$$F(q) = \int \rho(\vec{r})\ e^{i\vec{q}\cdot\vec{r}}\ d^3r.$$

A minor correction must be applied to Equation II-3 to account for recoil of the target nucleus [Ref. (8)].

Application of these principles to elastic electron scattering has yielded a great deal of information about both nucleon and nuclear ground state charge structure. However, this knowledge represents only a small portion of possible nuclear information since it bears only on the static properties of the ground state of the nucleus. The prospect of exciting the nucleus to higher energy levels in order to observe nuclear dynamics led to the study of inelastic electron scattering.

2. Inelastic Electron Scattering

Inelastic electron scattering is one of the most powerful tools available for nuclear structure studies. There are two basic reasons for this. First, the basic interaction is the well known electromagnetic interaction of the electron with the nuclear charge and current. Second, and more important, is the possibility of separately varying energy and momentum transfer (q), allowing mapping of the inelastic form factors of nuclear levels as a function of the momentum transfer [Ref. (7)].

Elastic scattering deals with ground state properties only. Inelastic scattering involves the excitation from the ground state to various excited states. When a relativistic, monoenergetic electron beam is incident on a thin (t << radiation length) target, a small fraction of the electrons will undergo collisions with nuclei. Use of a magnetic spectrometer capable of rotation about the scattering

axis enables the determination of the energy distribution of the scattered electrons at various angles. Most electrons are scattered elastically and appear in the spectrum as a sharp peak at an energy lower than the beam energy due to recoil, and with a width determined by overall experimental resolution. Below the elastic peak there appears in the spectrum of scattered electrons a continuous distribution called the radiation tail, which is due to bremsstrahlung. Superimposed on the radiation tail are peaks associated with nuclear excitation. All of the scattered electrons below the elastic peak have lost energy due to one or more energy exchange mechanisms. The experimentalist is only interested in those events involving the exchange of one photon from an electron to a nucleus, resulting in excitation of the nucleus. Therefore, all other energy exchange mechanisms must be understood well enough to accurately correct the inelastic spectra for proper observation of the superimposed nuclear resonances.

These corrections are most important for the elastic scattering, but they apply similarly to inelastic excitation. They fall into two categories: line shape corrections and radiative tail corrections. Line shape corrections arise since some of the scattered electrons are degraded in energy prior to being counted by the emission of soft photons, emission of a hard photon (bremsstrahlung), multiple collisions with nuclei, collisions with atomic electrons and

straggling due to ionization effects. These all lead to multiplicative factors, called radiative corrections, applied to the area under the elastic peak, which is proportional to the elastic cross section. The radiative tail is the energy distribution of the electrons which, by the processes just described, have been scattered out of the energy region of the elastic peak and form a continuous spectrum under the inelastic levels [Ref. (7)]. Naturally, each inelastic level has its own radiation tail which, for practical purposes, is mostly neglected in the evaluation.

Once the radiation tail and other experimental background have been subtracted, the remaining cross section consists of the inelastic cross sections corresponding to nuclear excitation levels. The analysis of how these cross sections depend on the scattering angle and therefore on momentum transfer q, gives the experimentalist a tool for studying nuclear structure and dynamics.

Since various physical parameters of the experimental arrangement are not known with sufficient accuracy, it has become customary in inelastic scattering to determine the ratio of inelastic to elastic cross section by measuring the inelastic peak area (A_{in}) relative to that of the elastic peak area (A_{el}), instead of doing absolute measurements. For targets of pure isotopes, this area ratio is proportional to the ratio of corresponding cross sections.

$$\left(\frac{d\sigma}{d\Omega}\right)_{in} = K\left(\frac{A_{in}}{A_{el}}\right)\left(\frac{d\sigma}{d\Omega}\right)_{el} , \qquad \text{(II-4)}$$

where K is a correction factor which accounts for: 1. differences in the radiative and ionization corrections of the elastic and inelastic peaks; 2. double or multiple scattering (more than one photon exchange); 3. the result of averaging the cross section over the spectrometer acceptance solid angle; and 4. any apparatus effects. Thus, the accuracy to which inelastic cross sections can be determined is limited by the experimental uncertainties of the peak area values and the precision to which the elastic cross section is known [Ref. (9)].

Equation (II-3) provides the nuclear form factor F(q) for elastic scattering from the theoretical and experimental cross sections. An analogous (but more complex) equation can be developed for inelastic scattering. The form factors in these equations contain information on the nuclear ground state for elastic scattering and on a given nuclear excitation level for inelastic scattering. To see this quantity more clearly, division of both sides of equation (II-4) by the Mott cross section yields

$$\frac{\left(\frac{d\sigma}{d\Omega}\right)_{in}}{\left(\frac{d\sigma}{d\Omega}\right)_{MOTT}} = C\,\frac{\left(\frac{d\sigma}{d\Omega}\right)_{el}}{\left(\frac{d\sigma}{d\Omega}\right)_{MOTT}} ,$$

where:

$$C = K \left(\frac{A_{in}}{A_{el}}\right) .$$

The use of such a relative cross section eliminates most of the kinematic factors, makes nuclear contributions more evident, and allows for more convenient presentation of the data in analogy to that of elastic scattering [Ref. (10)].

B. DISTORTED WAVE BORN APPROXIMATION

1. Cross Section Calculation

Actual computation of the cross section has become a more sophisticated procedure in recent years. Originally, the incoming and outgoing electron was treated in the Dirac formalism as a plane wave. In the Born approximation (or Plane Wave Born Approximation), the differential cross section can be written as a sum over the cross sections for electric (E) and Magnetic (M) multipole transitions [Ref. (9)]:

$$\left(\frac{d\sigma}{d\Omega}\right)_{PWBA} = \sum_{\lambda} \left(\frac{d\sigma}{d\Omega}\right)_{E\lambda} + \sum_{\lambda} \left(\frac{d\sigma}{d\Omega}\right)_{M\lambda} , \qquad \text{(II-6)}$$

where

$$\left(\frac{d\sigma}{d\Omega}\right)_{E\lambda} = \alpha^2 a_{\lambda} q^{2\lambda} k_o^{-2} [\lambda(\lambda+1)]^{-1} B(c\lambda, q, I_o \rightarrow I_x) V_L(\theta)$$

$$+ B(E\lambda, q, I_o \rightarrow I_x) V_T(\theta)] \; R^{-1}$$

and

$$\left(\frac{d\sigma}{d\Omega}\right)_{M\lambda} = \alpha^2 a_\lambda q^{2\lambda} k_o^{-2} B(M\lambda, q, I_o \rightarrow I_x) V_T(\theta) R^{-1} .$$

In the above

$$a_\lambda = 4\pi\lambda^{-1}(\lambda+1)[(2\lambda+1)!!]^{-2}$$

$$k_o = E_o/\bar{h}c$$

$$R = 1 + \bar{h}c(k_o/mc^2)(1 - \cos\theta)$$

λ = transition multipolarity

α = 1/137 = fine structure constant

E_o = primary electron energy

θ = scattering angle

m = nuclear mass.

However, steadily improving accuracy in electron scattering experiments has required more accurate analysis of data to obtain meaningful results. By modeling the incoming and outgoing electron as waves distorted by the Coulomb potential of the nucleus, this has been accomplished. An early publication of such an analysis dealing with elastic scattering was presented by Yennie and Ravenhall in 1954 [Ref. (11)]. Ravenhall used the model of the Dirac equation for an extremely relativistic electron in the elctrostatic potential of a static spherically symmetric charge distribution,

and found a new cross section obtained by a numerical calculation of the phase shift of each partial wave.

Electron scattering is concerned with high energy electrons ($E_i \gtrsim 30$ MeV) where the electron rest energy can be neglected ($m_o c^2$ is effectively zero). Therefore, the Dirac equation can be written as

$$(\vec{\sigma} \cdot \vec{p}c + V - E_i)\Phi = 0 \ , \qquad \text{(II-7)}$$

for which the scattering states have the asymptotic form

$$\Phi \sim \begin{pmatrix} 1 \\ 0 \end{pmatrix} e^{ikz} + r^{-1} f(\theta,\phi) \begin{pmatrix} 1 \\ \tan\frac{\theta}{2} e^{i\phi} \end{pmatrix} e^{ikr} \qquad \text{(II-8)}$$

which is the same for both spin orientations when V is a spherically symmetric potential. This can be decomposed into partial waves and summed:

$$\Phi = \Sigma \, a_{jm} \, \phi_{jm} \qquad \text{(II-9)}$$

where:

$$J^2 \, \phi_{jm} = j(j+1) \, \bar{h}^2 \, \phi_{jm}$$

and

$$J_z \, \phi_{jm} = m \, \bar{h} \, \phi_{jm}$$

with

$$\vec{J} = \vec{r} \times \vec{p} + \frac{1}{2} \vec{\sigma} \bar{h} .$$

By applying scattering theory at large distances from the scattering center and modifying the results to account for the long range effects of the Coulomb potential, the scattered wave becomes

$$\Phi_{SCATT} = X^{-1} k f(\theta) \left(\tan \frac{\theta}{2} e^{i\phi} \right) e^{i(x+\gamma \ln 2x)} \quad \text{(II-10)}$$

where

$$\gamma \equiv Z e^2/\bar{h}c$$

and

$$f(\theta) = \frac{1}{2ik} \Sigma e^{2i\eta_j} (j + \tfrac{1}{2}) (P_{j-\frac{1}{2}} + P_{j+\frac{1}{2}})$$

for

$$\theta \neq 0.$$

However, the phase shifts (η_j) do not approach a limit as j increases and therefore the summation of $f(\theta)$ is difficult and in practice is done using computer codes

[Ref. (11)]. Later, Rawitscher and Fischer modified the calculation to apply to cases where the energy is not in the extreme relativistic range [Ref. (12)].

Application of these principles to inelastic scattering is more involved and proceeded more slowly. The first successful computer codes for solving equations in the inelastic case was called GBROW and was described in a report by J. F. Ziegler [Ref. (13)]. Five conditions were assumed in GBROW:

1. Exchange of a single photon.
2. The transition is of a pure electric multipole character.
3. The nuclear ground state is spherically symmetric.
4. The excited state charge distribution is not significantly distorted from the ground state.
5. Nuclear recoil is negligible.

In this program the inelastic cross section is derived in the form of Fermi's Golden Rule:

$$\left(\frac{d\sigma}{d\Omega}\right)_{inel} = (\text{kinematic terms}) \sum_{m_i\, m_f} \left| \langle H_{int} \rangle_{f_i} \right|^2 \qquad \text{(II-11)}$$

where

$$H = H_o + H_{int}: \quad \begin{array}{l} H_o = \text{static interaction hamiltonian} \\ H_{int} = \text{dynamic interaction hamiltonian} \end{array}$$

and

$$\langle H_{int} \rangle_{fi} = \int_{\text{over nuclear volume}} \psi_f^{\dagger(N)} \text{(electron field)} \, \psi_i^{(N)} \, d\tau.$$

The integration is over the nuclear volume and $\psi_f^{(N)}$ and $\psi_i^{(N)}$ are the final and initial nuclear wave functions. Here the "electron field" is an expansion of the electron's electromagnetic field in partial waves.

Proceeding to separate Coulomb and current portions of the Dirac particle interaction, orienting the electron Z coordinate axis parallel to the incident electron direction, and using orthogonality relations between various spherical harmonic terms, the resultant cross section is

$$\left(\frac{d\sigma}{d\Omega}\right)_{\substack{\text{inel} \\ \text{DWBA}}} = \frac{V^2 E_i E_f P_f}{2(2\pi^2)\hbar^3 P_i} \frac{(2I_f + 1)}{(2I_i+1)(2L+1)} \Sigma \left| \langle H_{int} \rangle_{fi} \right|^2 \qquad \text{(II-12)}$$

where

V = normalization volume,

L = transition multipolarity,

and

$\langle H_{int} \rangle_{fi}$ is defined in [Ref. (13)].

If the cross section is written as in Equation (II-3), the form factor squared has the form (in Plane Wave Born Approximation)

$$|F|^2 = \{|F_{c,L}|^2 + (\tfrac{1}{2} + \tan^2 \tfrac{\theta}{2})[|F_{E,L}|^2 + |F_{M,L}|^2]\} \quad \text{(II-13)}$$

where $|F_{c,L}|^2$ is due to the Coulomb interaction only and is written

$$|F_{c,L}|^2 = \frac{1}{Z^2} \frac{4\pi}{[(2L+1)!!]^2} q^{2L} B(cL,q,J_i \to J_f) \ , \quad \text{(II-14)}$$

where

Z = atomic number

q = momentum transfer

$J_{i/f}$ = initial/final angular momentum of nucleus.

The transverse electric and magnetic terms are

$$|F_{\substack{E,L \\ M}}|^2 = \frac{4\pi}{Z^2} \left(\frac{L+1}{L}\right) \left[\frac{q^L}{(2L+1)!!}\right]^2 B(\substack{E \\ M}L,q,J_i \to J_f) . \quad \text{(II-15)}$$

The coefficients $B(X)$ in the above are the reduced nuclear transition probabilities. They now contain the desired information on a given level and are of the form

$$B(XL,q,J_i \to J_f) = \frac{1}{2J_i+1} |\langle J_f||\hat{M}(XL,q)||J_i\rangle|^2 \ , \quad \text{(II-16)}$$

where $\hat{M}$ represents the transition operator and will, in practice, contain a function representing the nuclear model used. In the distorted wave treatment, this function is the

nuclear model-dependent transition charge density operator $\rho_{tr}(r)$. Determination of spacial charge density functions $\rho_1(r), \rho_2(r), \rho_3(r)$ from this operator will then give an evaluation of the reduced transition matrix elements and enable the cross section calculation to be completed [Ref. (13)]. The model used in GBROW is the hydrodynamic model developed by Tassie [Ref. (14)]. The B-value is then defined and by $B(EL) = \int \rho_{tr}(r)\ r^2\ d\tau$ for electrical longitudinal transitions.

2. Tassie Model

It is customary to approach the actual calculation of the DWBA cross-section by first choosing an appropriate nuclear model and its associated transition charge density $\rho_{tr}(r)$ and transition currents j_N. The model is considered satisfactory if it furnishes computed cross section values that agree with the data. It has been found that for collective transitions (many particle excitation), reasonable agreement is obtained with the use of an oscillating liquid drop model described by Tassie [Ref. (14)]. This model is based on hydrodynamic vibrations of the nucleus. For collective excitations, transverse contributions to the cross-section are small below angles of about 150°, and can therefore be ignored without much loss of accuracy [Ref. (10) and (15)]. As presented by J. F. Ziegler in 1967 [Ref. (13)], the Tassie model transition charge density for a multipolarity L is [Ref. (14)]

$$\rho_L = r_N^{L-1} \frac{\partial \rho_o}{\partial r_N} . \qquad \text{(II-17)}$$

This form of ρ_{tr} is then entered into the DWBA calculations of the cross-section by the computer code GBROW.

C. GIANT RESONANCES

Prior to the development of inelastic electron scattering techniques, electromagnetic excitation of nuclear levels was studied mainly through photonuclear methods. A dominant feature of these spectra was known for years as "The Giant Resonance" or "Giant Dipole Resonance." This structure consistently appeared in spectra throughout the periodic table for excitation energies between 10 MeV and 25 MeV. Its absorption cross section exhausts approximately all of the classical Thomas-Reiche-Kuhn (TRK) dipole sum rule, which was originally derived for atomic excitations. It was therefore regarded as a strongly collective excitation in which a considerable number of nucleons participated. Through the use of monocromatic beams, produced by positron annihilation, very accurate results for excitation energy, width and line shape of the GDR were obtained [Ref. (16)].

During this period, electron scattering experiments were concerned mainly with investigations of the nuclear ground state, low level excitations and back scattering (180°) to isolate magnetic transitions, although some GDR studies were done in light nuclei. With the advent of better facilities, the investigation of giant resonances

in the nuclear continuum became possible. The first measurements covering nuclear excitations up to 28 MeV showed not only the GDR(E1) resonance in ^{140}Ce but also an E2 giant quadrupole resonance (GQR) below the GDR at 12.0 MeV which accounted for 65% of the E2 isoscalar sum rule and a giant magnetic dipole state (M1) at 8.7 MeV [Ref.s (3), (17)].

One of the characteristics of giant resonances is the relatively smooth dependence of their excitation energies (E_x) with the mass number, A. The use of a simple hydrodynamic nuclear model yields predictions of $E_x(GDR) \simeq 80A^{-1/3}$ for the GDR, close to the experimentally observed value in heavy nuclei. The GQR (E2) had been predicted earlier by Bohr and Mottelson [Ref. (18)] as an isoscalar collective E2 mode. Their predictions were

$$E_x(E2) = \frac{1}{\sqrt{2}} (2\hbar\omega_o) = 58A^{-1/3} \quad \text{(for the isoscalar E2)}$$

and

$$E_x(E2) = 135A^{-1/3} \quad \text{(for the isovector E2)}.$$

The isoscalar prediction of 11.2 MeV in ^{140}Ce compares favorably with the Darmstadt results of 12 MeV [Ref. (19)].

The discovery of the "new" giant resonances (GQR) in inelastic electron spectra results from the fact that the momentum transfer, q, can be varied independently of

excitation energy, E_x, in electron scattering. The γ-absorption cross section, for a given energy, can be measured only at $q = E/c$, which is called the photon point. However, in electron scattering, q can be varied over a wide range above the electron energy line by varying either the primary energy or the scattering angle, or both [Ref. (7)]. The governing equation for $q(E,\theta)$ is

$$q^2 = 4\ E_i\ E_f\ \sin^2\frac{\theta}{2}\ , \qquad \text{(II-18)}$$

where

$$E_{i/f} = \text{electron initial/final energy.}$$

By thus varying q, giant resonances with different multipolarities having different q dependence can be distinguished. Each of these resonances is associated with a particular value of angular momentum, L, transferred to the nucleus during the excitation. The GDR is an E1 mode corresponding to an L = 1 or dipole excitation. Experiments in many nuclei have produced evidence of E0, E2, E3 and M1 resonances within the nuclear continuum.

D. ^{89}Y EXPERIMENTAL SURVEY

For comparison to the present measurements, a survey was made of previous experiments with ^{89}Y, for which there have been fewer experiments than with other nuclei in this

mass range. Initial efforts were directed towards an ^{88}Sr core with an extra proton [Refs. (20, (21) and (22)] but the weak coupling model could not adequately describe the excited states. Continued effort was almost strictly in the 0 to 4 MeV range and is tabulated by date in Table I.

In the giant resonance region, a radiative proton capture reaction $^{89}Y(p,\gamma_o)^{90}Zr$ determined the existence of giant E1 excitations in ^{90}Zr at E_x = 16.5 MeV with a width of Γ = 4 MeV [Ref. (23)]. Using (e,e'), Fukuda and Torizuka measured E1 at E_x = 16.65 MeV and Γ = 4.0 MeV in ^{90}Zr. The latter experiment also reported an E2 at E_x = 14.0 MeV and Γ = 4.8 MeV and at E_x = 27MeV. All fits were made using Lorentz line shapes. Here, incident electrons of 150 to 250 MeV were scattered at angles of 35° and 45° specifically so that the longitudinal terms would dominate the excitation function. Youngblood [Ref. (24)] reported an E2 giant resonance found in ^{90}Zr using α particle scattering at E_x = 14.5 ± .3 with width Γ = 4.0 ± .2. This resonance took up 56% ± 17% of the E2 sum rule.

In an as yet unpublished paper [Ref. (25)], Bertrand has reported an isoscalar giant quadrupole resonance E2 in ^{89}Y at E_x = 13.8 ± .2 MeV of width Γ = 3.32 MeV. These results are from an (p,p') experiment and contain 24% ± 5% of the energy weighted sum rule. The measurements were taken at Oak Ridge National Laboratory.

A compilation of photonuclear experiments by Berman [Ref. (16)] gives data on the giant dipole resonance E1 at E_x = 16.77 MeV and Γ=4.1 MeV. This data compares favorably with the present work.

TABLE I. PREVIOUSLY REPORTED TRANSITIONS

ENERGY (MEV)	WIDTH (MEV)	TYPE EXPERIMENT	REFERENCE
1.50	RES	(N,N'γ)	20
		(α, α')	26
		(P,P')	21
		(E,E')	22
1.74	RES	(N,N'γ)	20
		(α, α')	26
		(P,P')	21
		(E,E')	22
2.21	RES	(N,N'γ)	20
		(P,P')	21
		(E,E')	22
2.52	RES	(N,N'γ)	20
		(P,P')	21
		(E,E')	22
2.86	RES	(N,N'γ)	20
		(E,E')	22
	DOUBLET	(P,P')	27
3.1	RES	(N,N'γ)	20
		(E,E')	22
	TRIPLET	(P,P')	27
3.72	RES	(E,E')	22
4.0	RES	(E,E')	22
4.46	RES	(E,E')	22
13.8+.2	3.2	(P,P')	25
16.79	3.95	(γ, γ')	28
16.74	4.25	(γ, γ')	29

NOTE: RES = RESOLUTION

III. DATA ACQUISITION

A. EXPERIMENTAL PROCEDURES

The physical layout and operational procedures of the NPS LINAC have been well documented [Refs. (30) and (31)]. A major improvement has occurred in the meantime with the installation of ion vacuum pumps to replace oil diffusion pumps in much of the vacuum system. Extensive acid cleaning of the wave guides to remove oil deposits was performed before the completion of the vacuum pump replacement. This change resulted in more reliable operation of the LINAC.

Several runs were made prior to the actual data acquisition in an effort to check and reduce background in the counting system. Of the four angles measured, the 105° measurement had the least background, because of extensive extra shielding added to the beam pipe just following the deflection magnets and prior to the target chamber. Fluctuations in the data were also reduced by improvements to the counting system beam current monitor. This device is designed to shut off the counting system whenever the analyzed beam current falls below a preset value.

Two C^{12} target calibration runs were made to calibrate the magnetic spectrometer by checking the measured excitation energy of the 15.1 MeV state.

B. DATA ACCUMULATION

A total of seven experimental runs were made using 92.5 MeV incident electrons scattering at 75°, 90°, 105° and 120° deflection angles. The scattered electron energies were measured from 96 to 50 MeV in 0.1 MeV steps. Targets with a width of 180 mg/cm^2 and 280 mg/cm^2 were used. The procedures for all runs were identical to those described in Ref. [(31)].

C. DATA REDUCTION

The single counter spectra for the ten counters of the counter ladder were collected by means of a teletype printer and tape punch unit. The tape was compiled and read onto magnetic tape by use of the NPS Digital Equipment Corporation PDP11-50 Duplex System. This tape was then read onto the NPS Computer Center IBM 360/67 time-sharing system for text editing and data reduction purposes. The final spectrum was then stored on the mass storage (Data Cell) of the OS System for further evaluation. Determination of the resonances which make up the inelastic spectrum was accomplished with a line shape fit program. The elastic line shape was assumed to be made up of two Gaussian curves both with the same height but different widths, which were joined to a short radiation tail of assumed hyperbolic shape. The elastic cross section, thus calculated, was then used to calculate the radiation tail and inelastic cross section (see Section II.A.2., eqs. II-4, II-12).

As a result of the comparison of Breit-Wigner forms to Lorentz forms in Ref. [(32)], and the better fits experienced with the former, Breit-Wigner line shapes were used for the resonance fits. The photonuclear work described in Section II.D. gives the parameters for the E1 resonance, E_x = 16.77 and Γ = 4.1 MeV, which were used as a starting point. The B-value of the E1 resonance can be calculated from the integrated cross section by using the formula [Ref. (15)]

$$\int \sigma_\gamma \, dE = \pi^2 \bar{\hbar} c \alpha \frac{8\pi(L+1)}{[(2L+1)!!]^2} k^{2L-1} B(L,k) \quad . \qquad \text{(III-1)}$$

The peak height of the E1 resonance in the different spectra was then chosen to reproduce the calculated B-value of 19.7 fm^2.

The following criteria to determine a reasonable fit were used:

(1) The data and calculated spectrum should coincide visually.

(2) The χ^2 per degree of freedom should be less than one. The errors are not strictly statistical because the detector momentum interval is larger than the momentum increment of the spectrometer field and hence correlations exist between energy bins.

(3) All observed resonances and widths must consistently fit spectra for all angles. The high background and low counts obtained at 120° made that data comparably erratic and the results less reliable despite the relatively low χ^2.

Figures 1 through 4 show the experimental inelastic spectra with the fitted total background and the individual resonances superimposed. Figures 5 through 8 show the corresponding spectra with the radiation tail subtracted revealing the resonance structures more clearly.

Inelastic form factors squared, F^2, for each resonance are computed by the **fit** program, as reported in Ref. [(33)], using

$$|F_i|^2 = \left(\frac{A_i}{A_{el}}\right) |F_{el}|^2 \qquad \text{(III-2)}$$

where F_i = inelastic form factor for resonance

A_i = area under resonance

A_{el} = area under elastic peak

F_{el} = elastic form factor.

B(EL) values are calculated with the form factor squared as calculated with DWBA, where

$$B(EL) = \frac{F_i^2}{F_{DWBA}^2} \quad . \qquad \text{(III-3)}$$

Tables II through V give the form factor squared and B value for each resonance at each angle. Figures 9 and 10 give the angular dependence of the squared form factor for the electric and the magnetic multipolarities with the curves normalized to the same maximum height. These curves were

used in making multipolarity assignments as shown in Figures 11 through 20.

Table VI presents the compiled resonances determined, their energies, widths, B values and multipolarity assignments. Energy weighted sum rule per cent and single particle unit calculations are presented for each resonance in Table VII.

D. ERROR ANALYSIS

As line shapes for each of the resonances were fit to the four spectra of 75°, 90°, 105° and 120°, obvious variations in energy location and widths were noted. These variations were limited to approximately 200 KeV in both energy and width while still maintaining reasonable χ^2's. A definite correlation was noted between radiation tail subtraction changes in the fit program and the resulting transition strength form factor squared outputs. Table VI shows the largest deviation from the average values of resonance energies, widths and form factors of the four angles for each resonance. The reasons for these relatively large errors including statistical fluctuations, equipment functional variance and operator error. Warshawsky and Weber [Ref. (31)] report the various LINAC equipment and operator contributions to errors. The repeatability of the 90° and 120° spectra both indicate considerable improvement in the stability of the LINAC, as compared with Ref. 31. To determine the statistical error of the average reduced

transition matrix element, a weighted B(EL)-value was computed using each of the four spectrum values.

$$\bar{B}(EL) = \frac{\sum_i B_i(EL)/(\Delta A_i)^2}{\sum_i 1/(\Delta A_i)^2}$$

where: $i = 75°, 90°, 105°, 120°$

ΔA_i = peak area statistical error from the fit program.

The statistical error of this weighted average B(EL)-value is then

$$\Delta\bar{B}(EL) = \frac{\bar{B}(EL)}{\sum_i 1/(\Delta A_i)^2} \quad .$$

These errors were consistently less than 1% of the computed $\bar{B}(EL)$ values, much less than the variance of the B_i. Hence, this statistical error was mainly used to calculate $\bar{B}$.

The total error given in Table VI is a rounded combination of the statistical error and a best estimate obtained from fluctuations in the value of the form factor squared experienced during the fitting process. These errors ranged from 10 to 30%.

TABLE II. RESONANCES AT 75° SCATTERING ANGLE

E (MEV)	Q (FM^{-1})	XL	FORM FACTOR SQUARED	B VALUE (*)
6.60	.553	E2	$2.37X10^{-4}$	$3.11X10^{2}$
		M1		$3.59X10^{0}$
8.09	.549	E2	$2.76X10^{-4}$	$3.62X10^{2}$
		M1		$4.06X10^{0}$
9.80	.544	E2	$8.77X10^{-5}$	$1.15X10^{2}$
11.15	.540	E2	$6.63X10^{-5}$	$8.70X10^{1}$
		E0		$1.54X10^{2}$
12.60	.536	E3	$3.94X10^{-5}$	$6.11X10^{3}$
		M2		$3.15X10^{1}$
13.50	.534	M2	$7.71X10^{-5}$	$6.27X10^{1}$
		E3		$1.19X10^{4}$
14.60	.526	E2	$2.53X10^{-4}$	$3.32X10^{2}$
16.60	.526	E1	$7.19X10^{-4}$	$1.97X10^{1}$
27.70	.500	E2	$4.71X10^{-4}$	$6.36X10^{2}$

* UNITS: $e^{2}FM^{2L}$ FOR ELECTRIC

$e^{2}FM^{2L-2}$ FOR MAGNETIC

TABLE III. RESONANCES AT 90° SCATTERING ANGLE

E (MEV)	Q (FM^{-1})	XL	FORM FACTOR SQUARED	B VALUE (*)
6.75	.640	E2	$1.60X10^{-4}$	$2.52X10^{2}$
		M1		$4.57X10^{0}$
8.20	.635	E2	$2.05X10^{-4}$	$3.19X10^{2}$
		M1		$5.62X10^{0}$
10.20	.628	E2	$4.10X10^{-5}$	$6.21X10^{1}$
11.25	.625	E2	$5.32X10^{-5}$	$8.00X10^{1}$
		E0		$1.44X10^{2}$
12.50	.621	E3	$5.33X10^{-5}$	$5.83X10^{3}$
		M2		$3.58X10^{1}$
13.60	.617	M2	$1.02X10^{-4}$	$6.87X10^{1}$
		E3		$1.13X10^{4}$
15.00	.612	E2	$3.04X10^{-4}$	$4.39X10^{2}$
16.60	.607	E1	$3.84X10^{-4}$	$1.97X10^{1}$
28.10	.572	E2	$3.42X10^{-4}$	$4.60X10^{2}$

* UNITS: $e^{2}FM^{2L}$ FOR ELECTRIC

$e^{2}FM^{2L-2}$ FOR MAGNETIC

TABLE IV. RESONANCES AT 105° SCATTERING ANGLE

E (MEV)	Q (FM^{-1})	XL	FORM FACTOR SQUARED	B VALUE (*)
6.69	.718	E2	$1.16X10^{-4}$	$2.70X10^{2}$
		M1		$8.86X10^{0}$
8.05	.713	E2	$1.41X10^{-4}$	$3.20X10^{2}$
		M1		$1.02X10^{1}$
10.15	.705	E2	$6.08X10^{-5}$	$1.31X10^{2}$
11.35	.700	E2	$4.24X10^{-5}$	$8.86X10^{1}$
		E0		$1.60X10^{2}$
12.45	.696	E3	$3.57X10^{-5}$	$3.57X10^{3}$
		M2		$2.37X10^{1}$
13.60	.691	M2	$9.29X10^{-5}$	$6.15X10^{1}$
		E3		$9.29X10^{3}$
14.85	.687	E2	$2.37X10^{-4}$	$4.59X10^{2}$
16.60	.680	E1	$1.71X10^{-4}$	$1.97X10^{1}$
27.80	.639	E2	$3.06X10^{-4}$	$4.81X10^{2}$

* UNITS: $e^2 FM^{2L}$ FOR ELECTRIC

$e^2 FM^{2L-2}$ FOR MAGNETIC

TABLE V. RESONANCES AT 120° SCATTERING ANGLE

E (MEV)	Q (FM^{-1})	XL	FORM FACTOR SQUARED	B VALUE (*)
6.73	.783	E2	$1.25X10^{-4}$	$5.45X10^{2}$
		M1		$1.03X10^{1}$
8.00	.778	E2	$1.60X10^{-4}$	$6.41X10^{2}$
		M1		$1.42X10^{1}$
9.90	.770	E2	$3.10X10^{-5}$	$1.15X10^{2}$
11.10	.765	E2	$2.02X10^{-5}$	$7.18X10^{1}$
		E0		$1.31X10^{2}$
12.30	.759	E3	$5.08X10^{-5}$	$5.29X10^{3}$
		M2		$3.68X10^{1}$
13.80	.753	M2	$9.17X10^{-5}$	$6.50X10^{1}$
		E3		$9.55X10^{3}$
15.00	.748	E2	$9.83X10^{-5}$	$3.00X10^{2}$
16.60	.741	E1	$1.08X10^{-4}$	$1.97X10^{1}$
27.80	.695	E2	$2.71X10^{-4}$	$5.52X10^{2}$

* UNITS: $e^{2} FM^{2L}$ FOR ELECTRIC

$e^{2} FM^{2L-2}$ FOR MAGNETIC

TABLE VI. COLLECTIVE RESONANCES AND IDENTIFICATIONS

E (MEV)	ERROR (MEV)	Γ (MEV)	ERROR (MEV)	B VALUE (*)	TOTAL ERROR %	MULTIPOLARITY
6.69	.09	.97	.13	$(2.96\pm.01)10^{2}$	20	E2
				$(6.10\pm.01)10^{0}$	20	M1
8.09	.12	1.22	.22	$(3.48\pm.01)10^{2}$	10	E2
				$(6.82\pm.01)10^{0}$	10	M1
10.01	.21	1.23	.17	$(1.11\pm.01)10^{2}$	10	E2
11.21	.14	1.50	0	$(8.45\pm.07)10^{1}$	30	E2
				$(1.59\pm.01)10^{2}$	30	E0
12.46	.16	1.14	.11	$(5.23\pm.03)10^{3}$	20	E3
				$(3.23\pm.02)10^{1}$	20	M2

* UNITS: $e^{2}FM^{2L}$ FOR ELECTRIC

$e^{2}FM^{2L-2}$ FOR MAGNETIC

TABLE VI. CONTINUED

E (MEV)	ERROR (MEV)	Γ (MEV)	ERROR (MEV)	B VALUE (*)	TOTAL ERROR %	MULTIPOLARITY
13.63	.17	1.20	.10	$(6.48\pm.01)10^{1}$	20	M2
				$(9.99\pm.02)10^{3}$	20	E3
14.86	.26	3.03	.07	$(4.23\pm.01)10^{2}$	20	E2
16.60	0	4.10	0	1.97×10^{1}	0	E1
27.85	.25	6.90	.10	$(5.46\pm.01)10^{2}$	30	E2

* UNITS: $e^2 FM^{2L}$ FOR ELECTRIC

$e^2 FM^{2L-2}$ FOR MAGNETIC

TABLE VII. SUM RULES AND SINGLE PARTICLE TRANSITION STRENGTHS FOR ^{89}Y

E (MEV)	XL	EWSR %	B (SPU)	E ($A^{-1/3}$ MEV)
6.69	E2	7.7±1.6	2.5	30
8.09	E2	11.0±2.2	2.9	36
10.01	E2	4.3±0.4	0.9	45
11.21	E2	3.7±1.1	0.7	50
12.46	E3	3.5±0.7	1.6	56
13.63	M2		35.4	61
14.86	E2	24.6±4.9	3.6	66
16.60	E1	100.6±0.1	5.1	74
27.88	E2	46.3±13.9	4.6	125

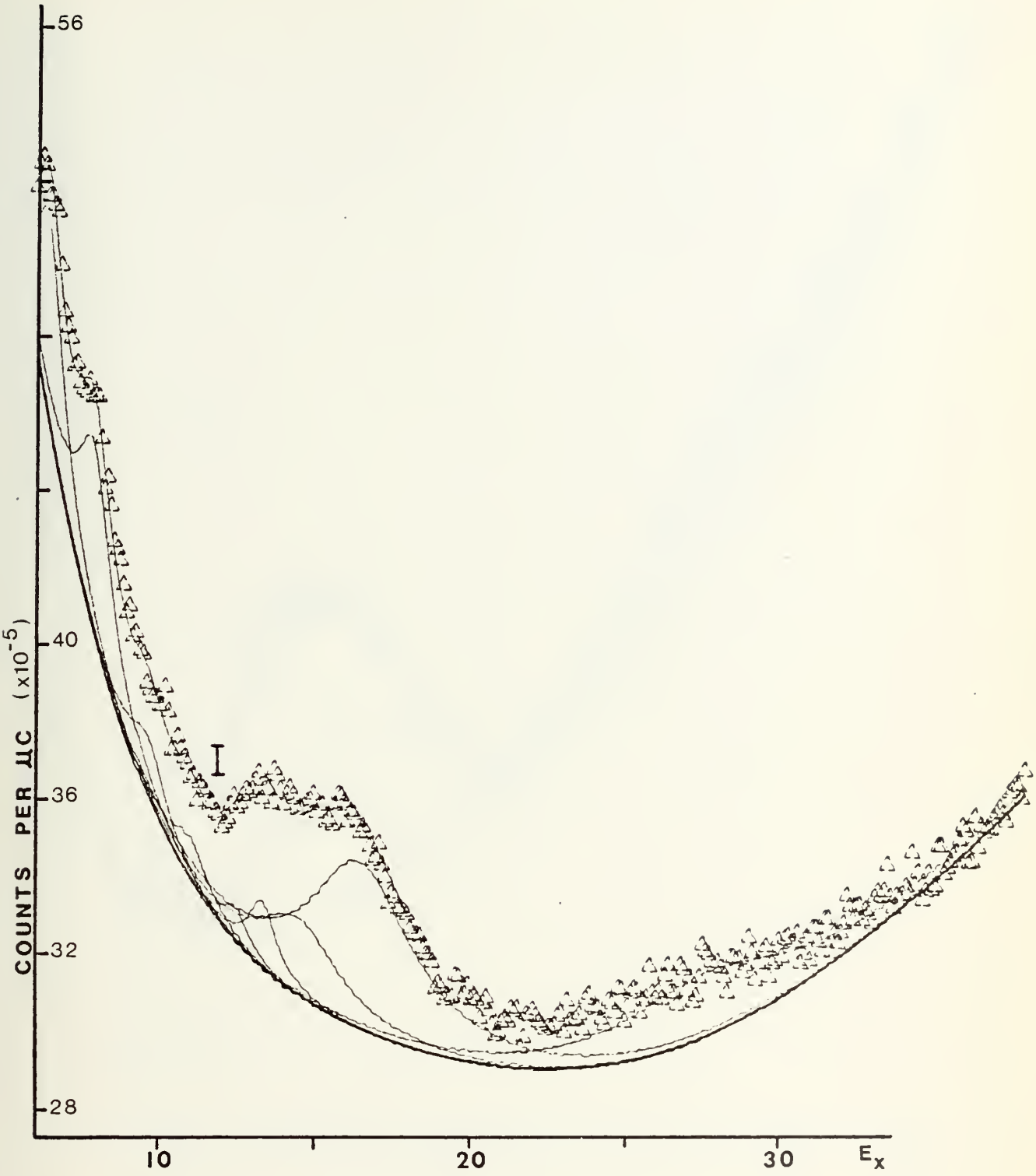

FIGURE 1. 75° Spectrum with background

FIGURE 2. 90° Spectrum with background

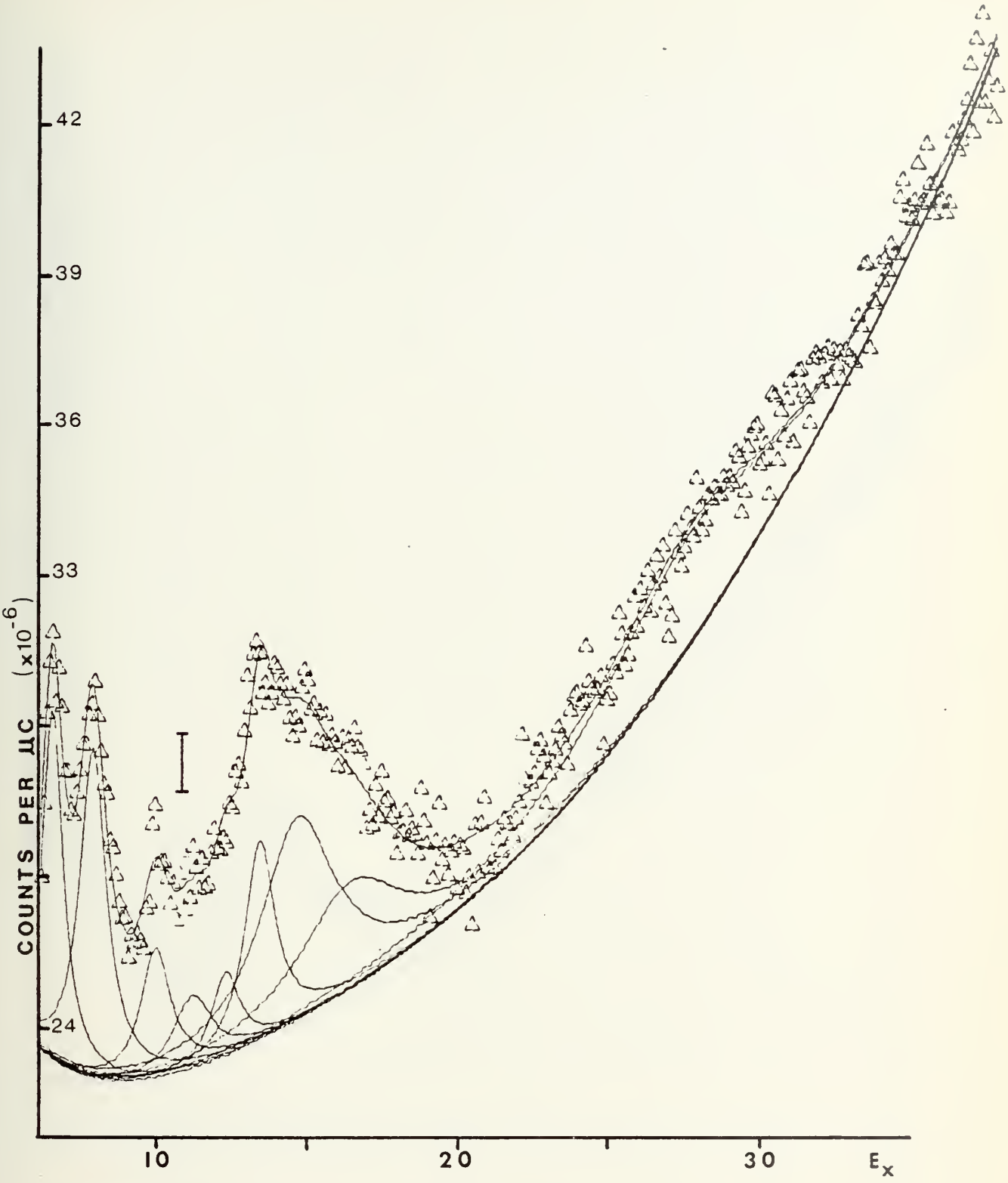

FIGURE 3. 105° Spectrum with background

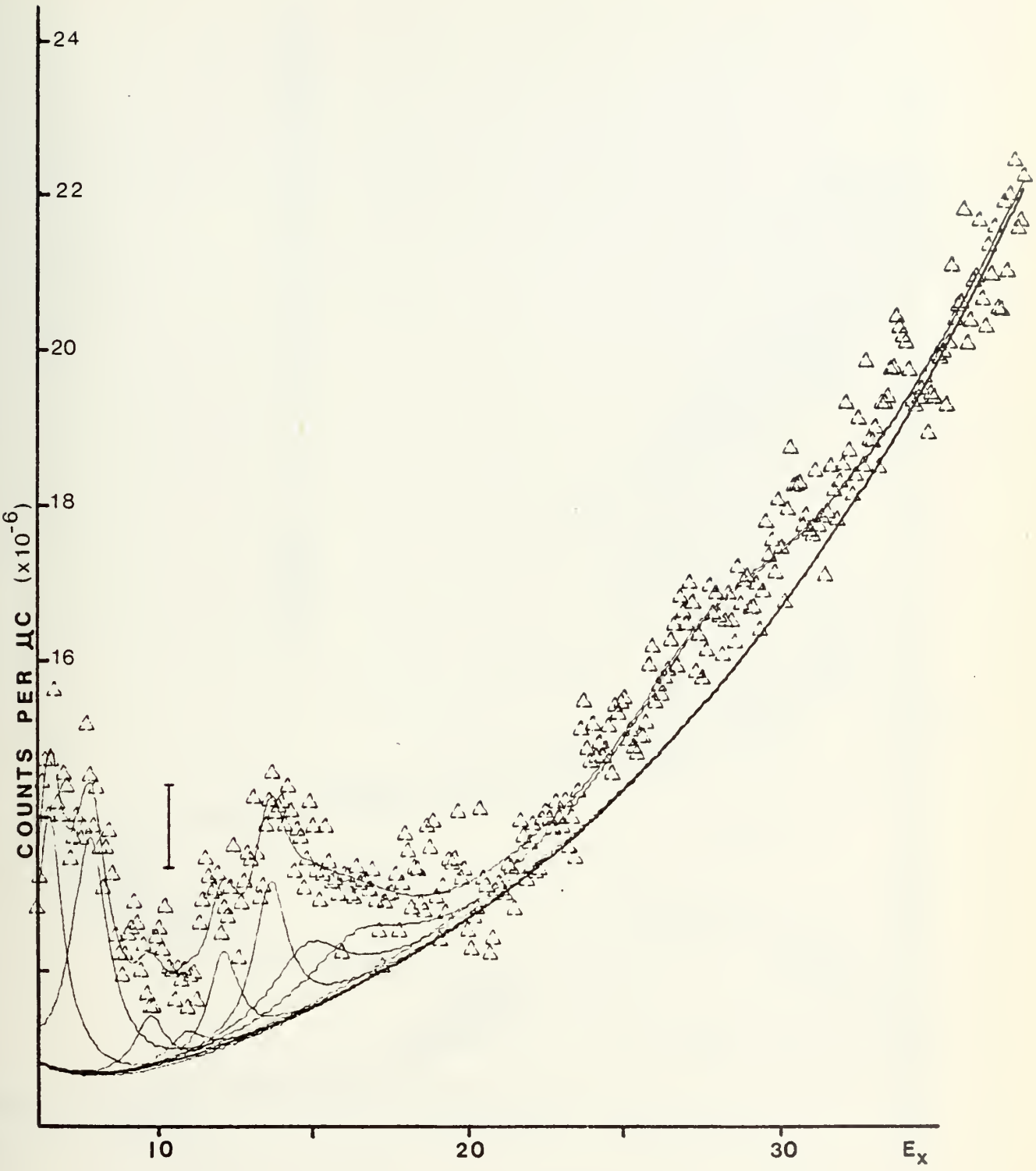

FIGURE 4. 120° Spectrum with background

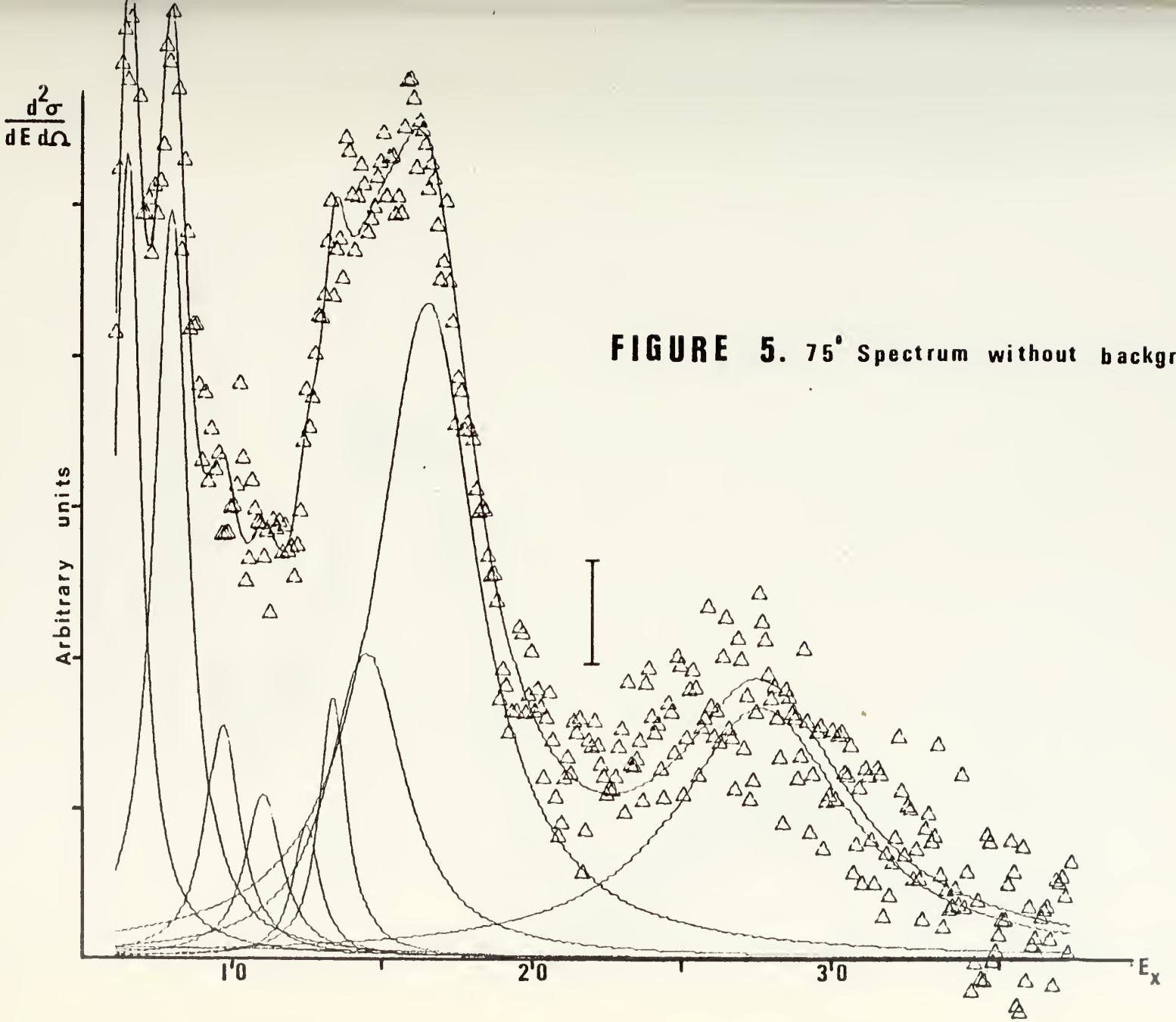

FIGURE 5. 75° Spectrum without background

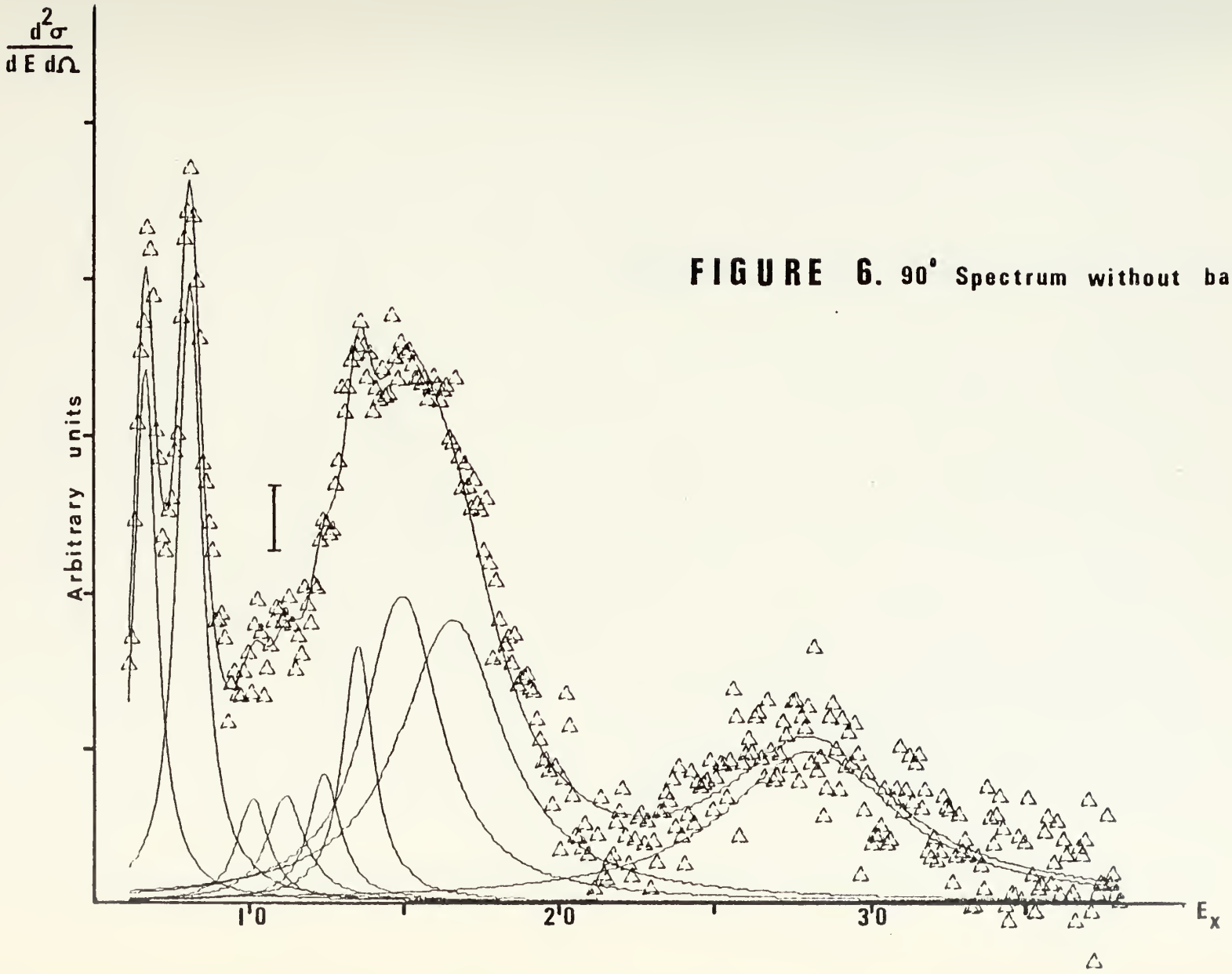

FIGURE 6. 90° Spectrum without background

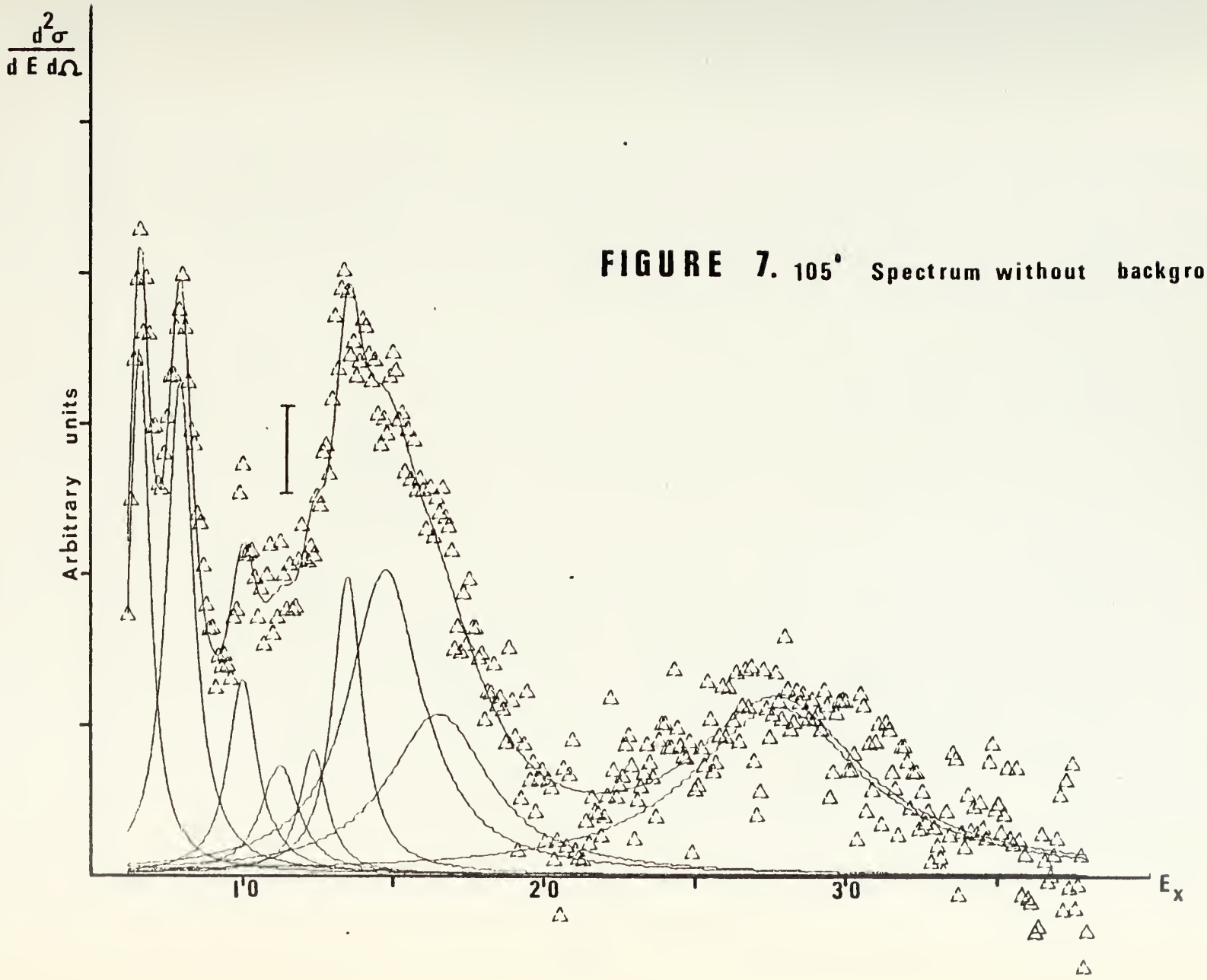

FIGURE 7. 105° Spectrum without background

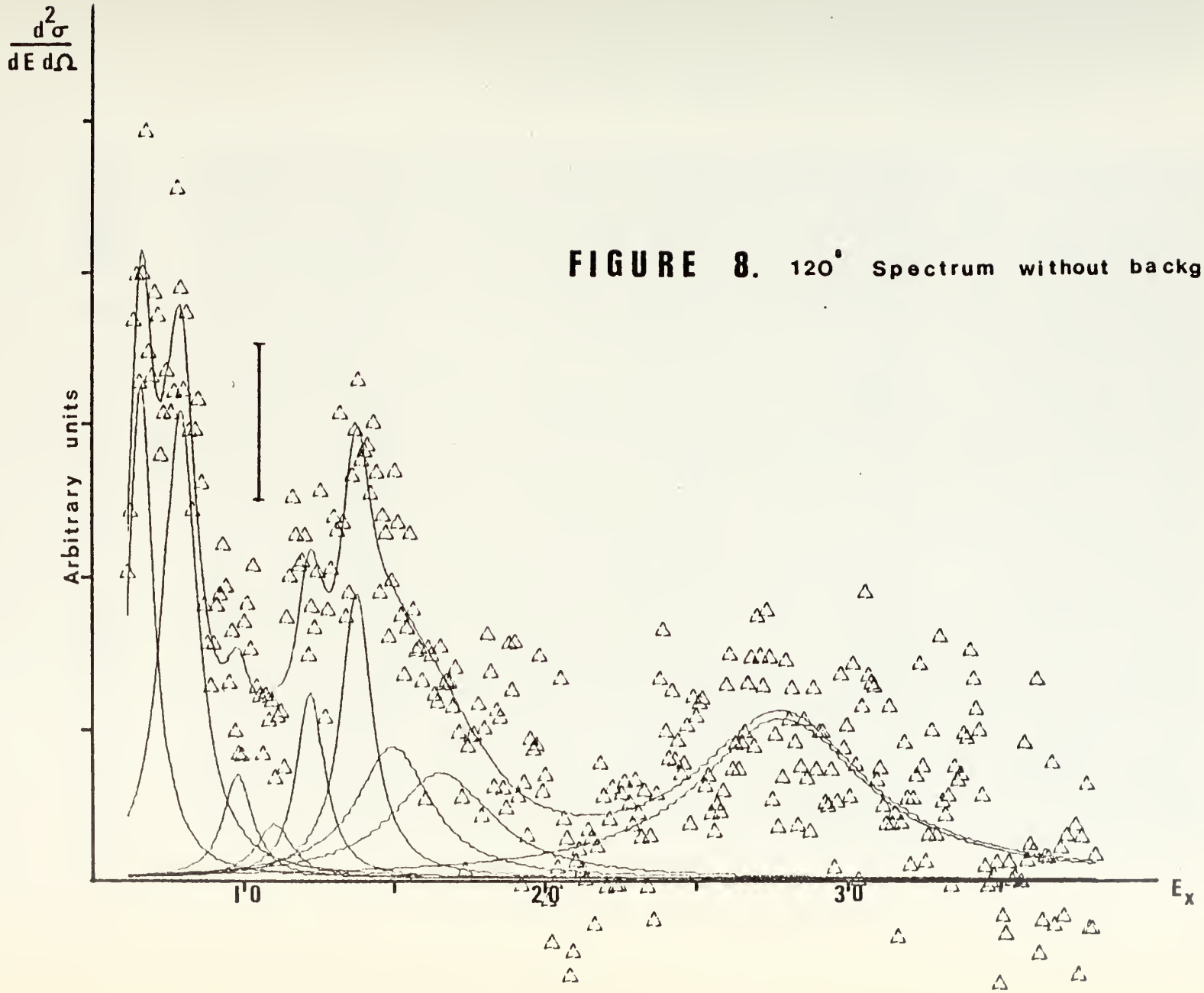

FIGURE 8. 120° Spectrum without background

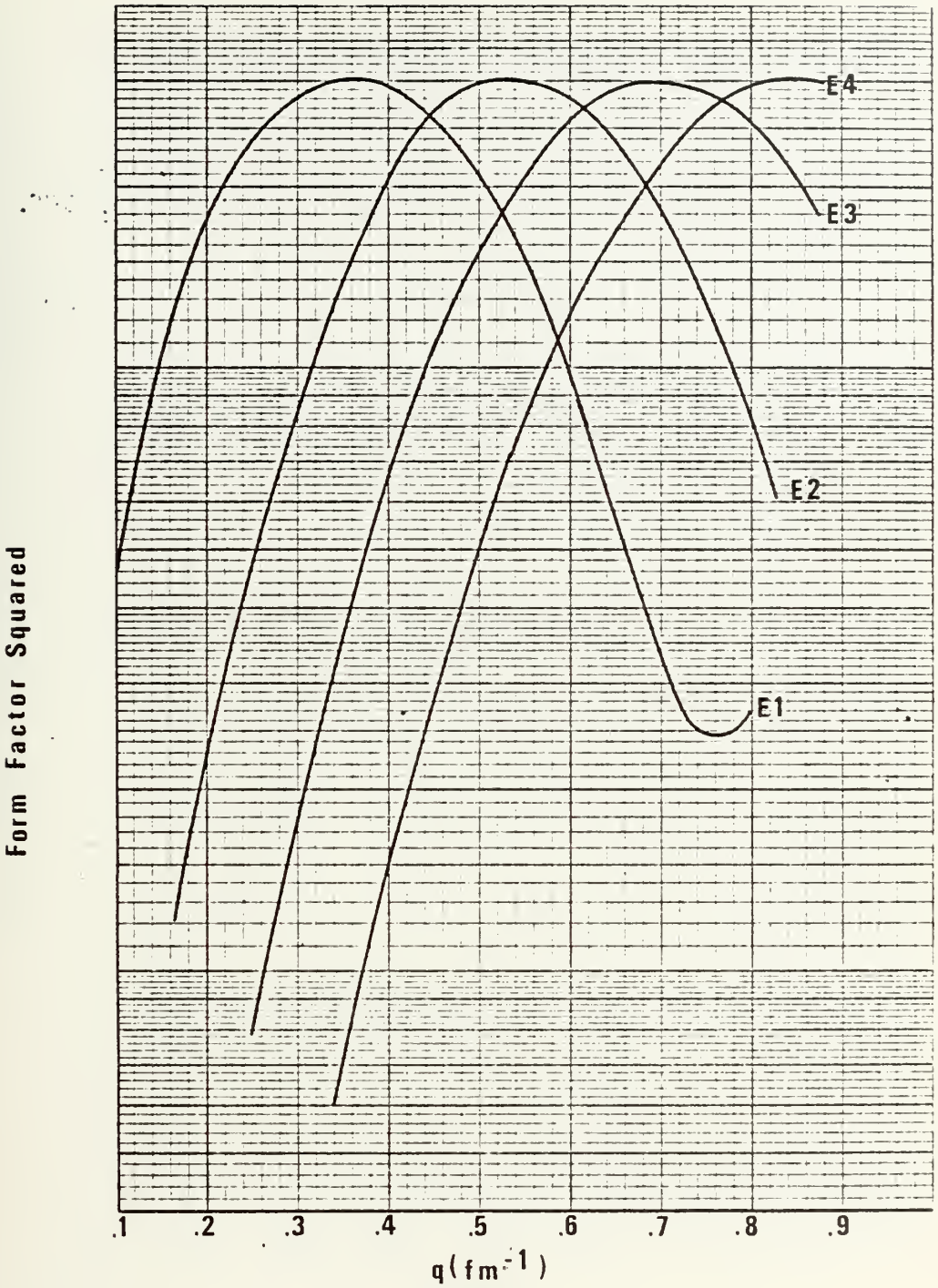

FIGURE 9. E1 - E4 Form Factors in comparison

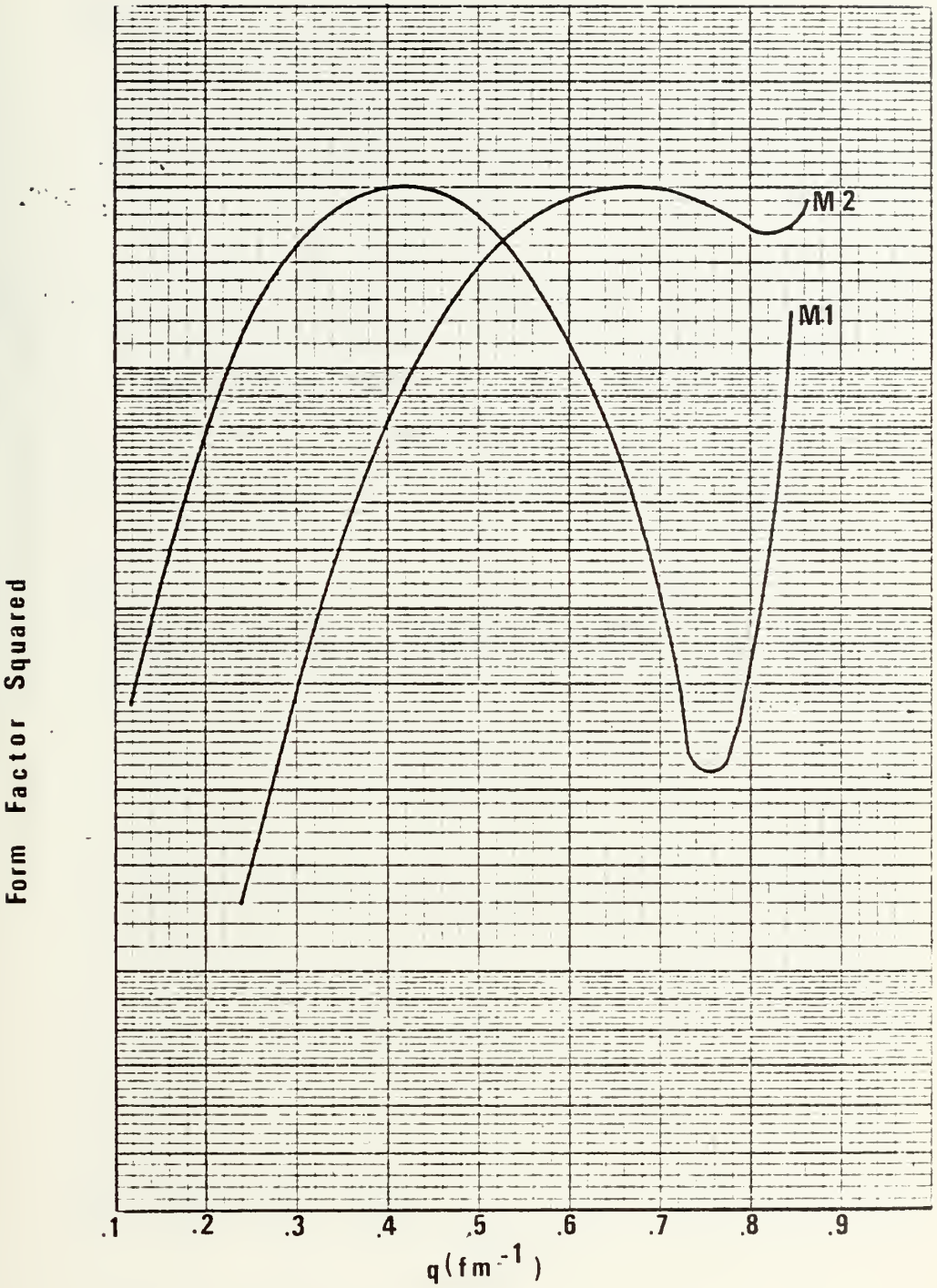

FIGURE 10. M1 - M2 Form Factors in comparison

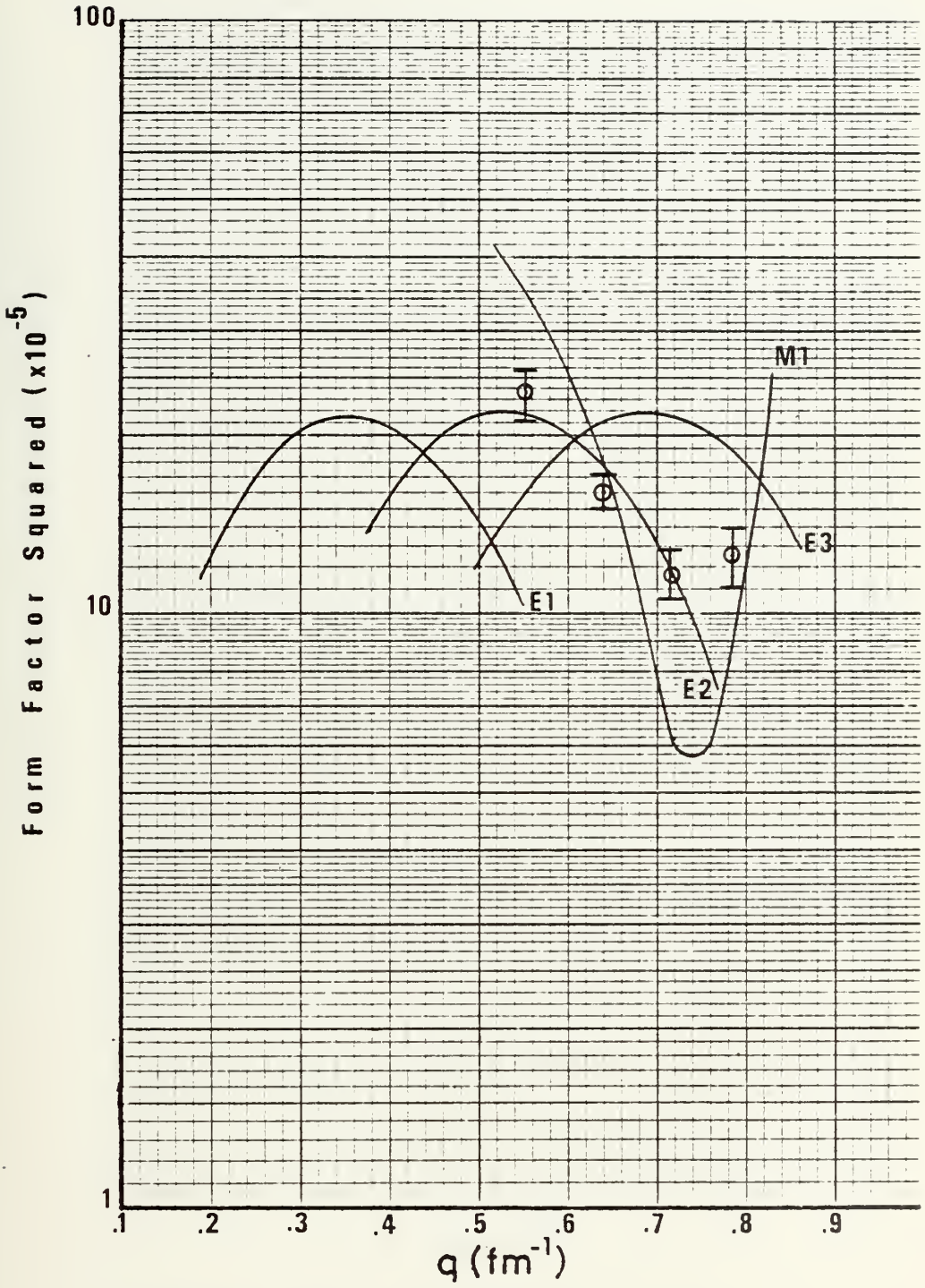

FIGURE 11. Experimental inelastic form factors for state at 6.69 MeV

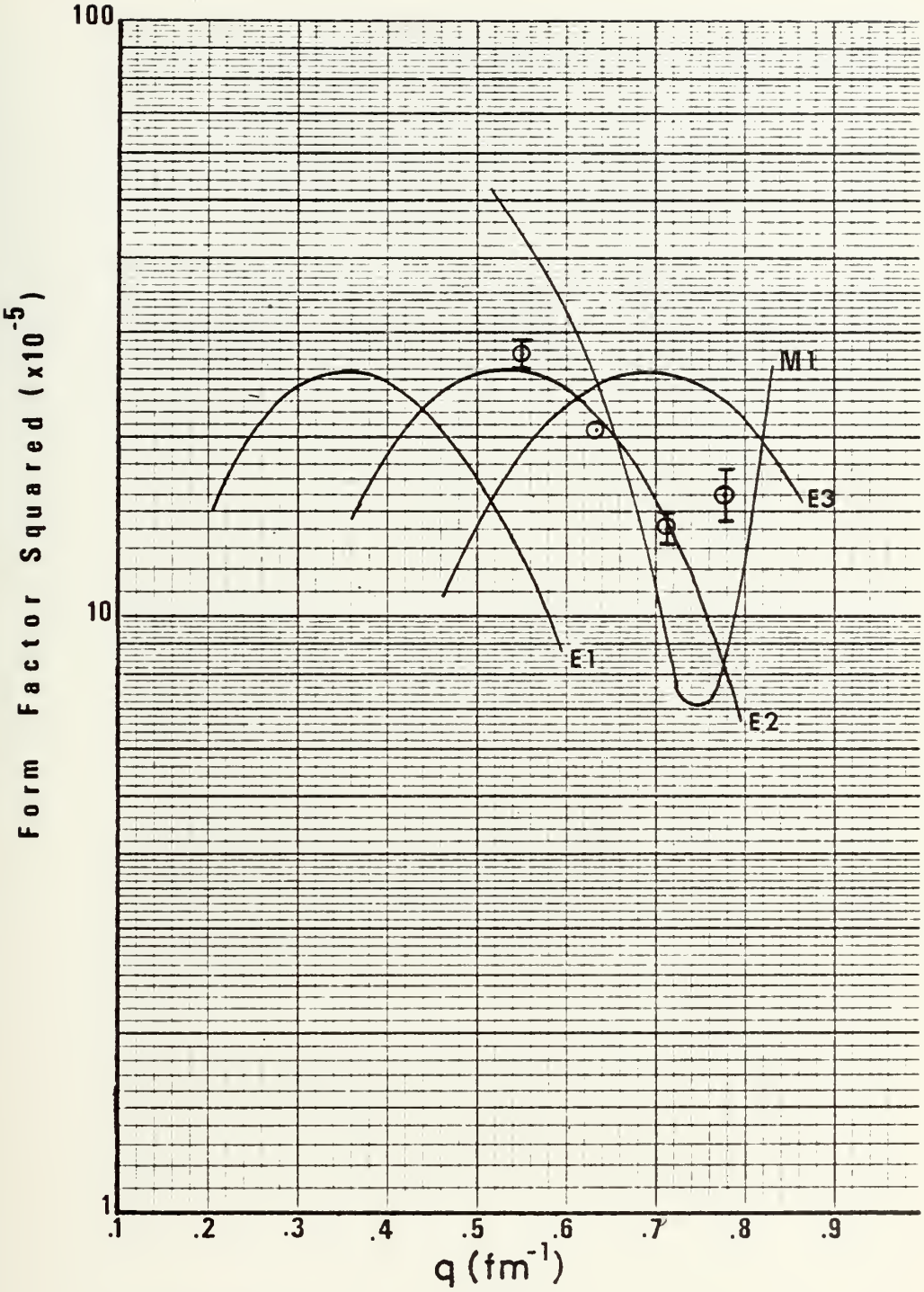

FIGURE 12. Experimental inelastic form factors for state at 8.09 MeV

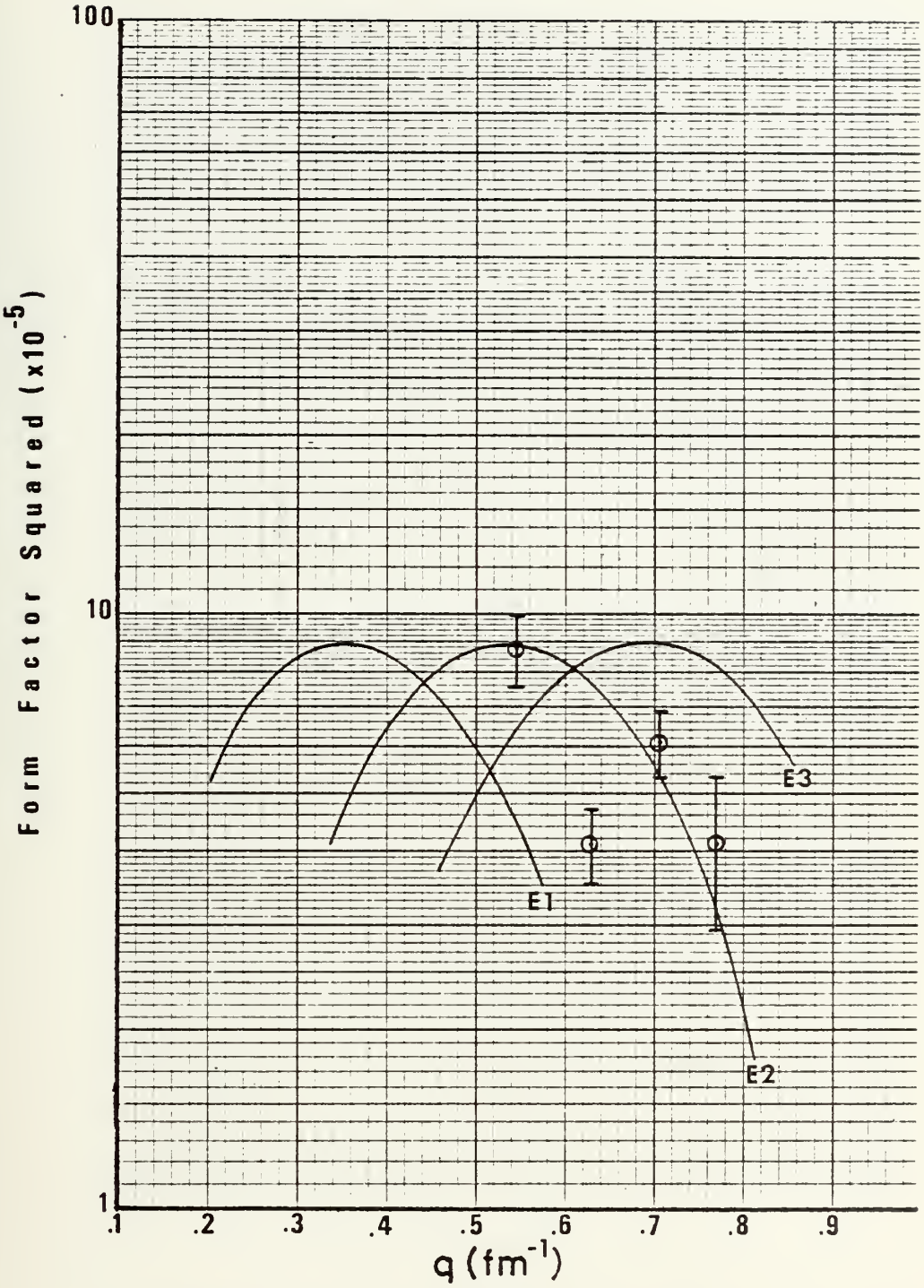

FIGURE 13. Experimental inelastic form factors for state at 10.01 MeV

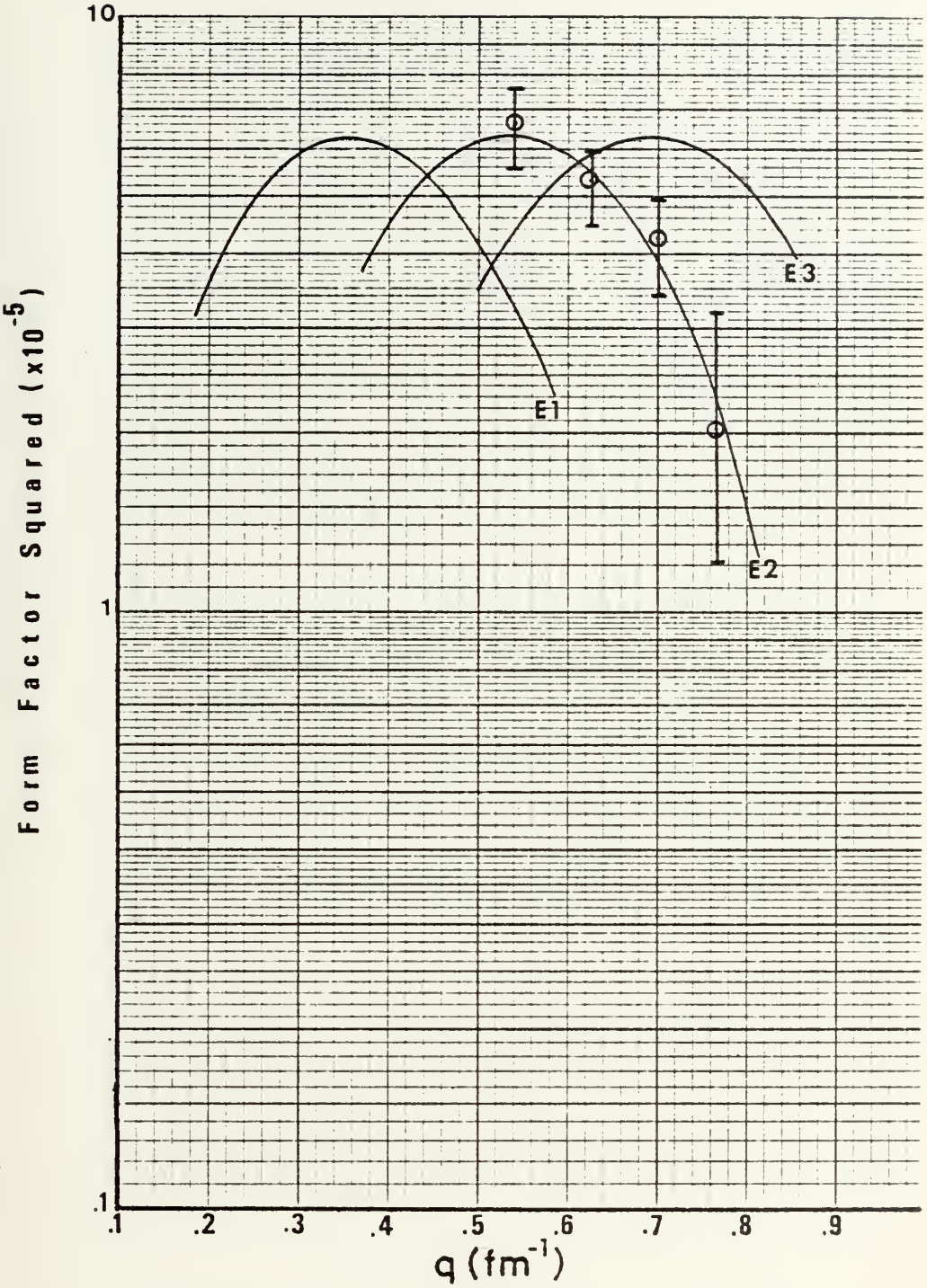

FIGURE 14. Experimental inelastic form factors for state at 11.21 MeV

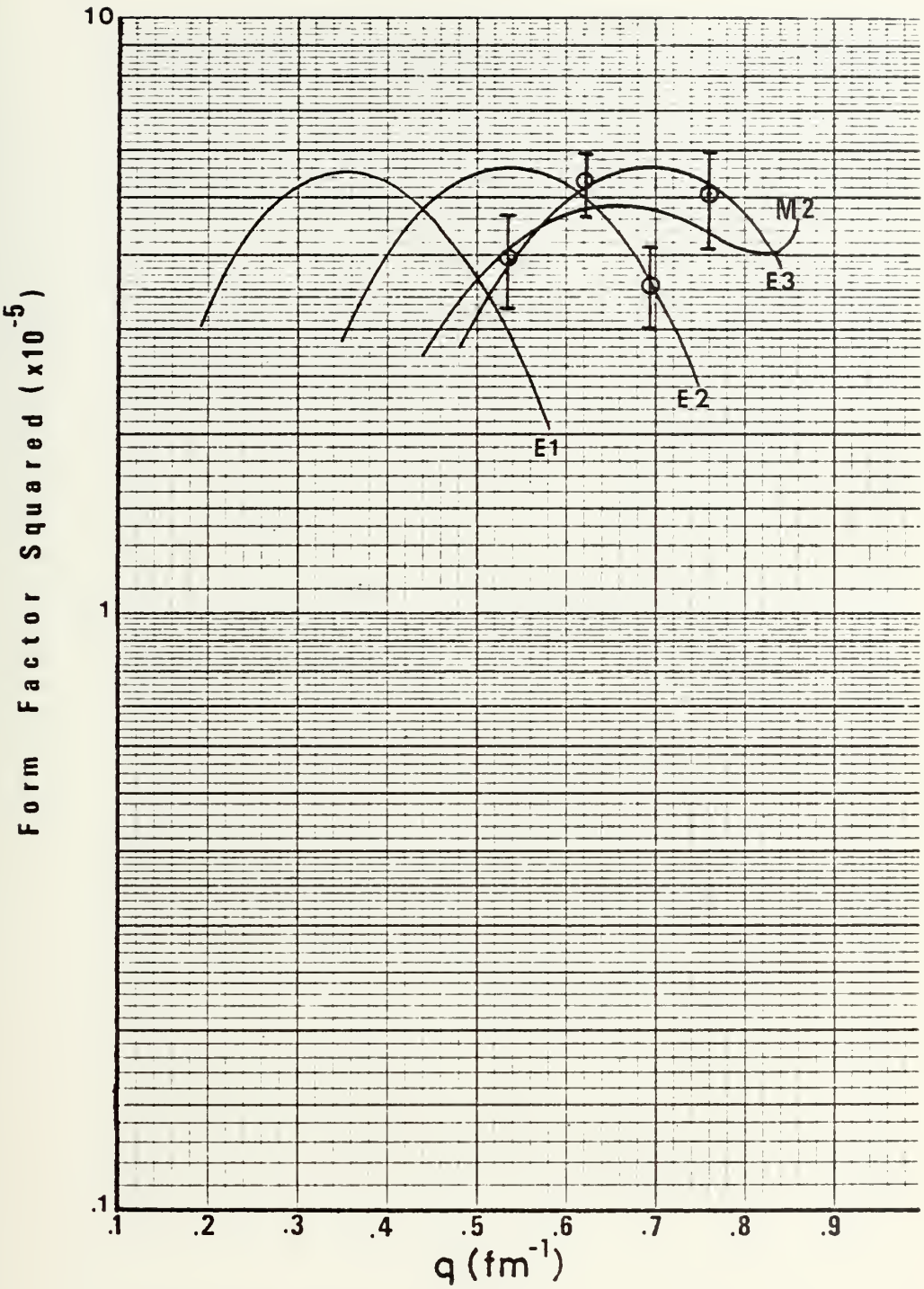

FIGURE 15. Experimental inelastic form factors for state at 12.46 MeV

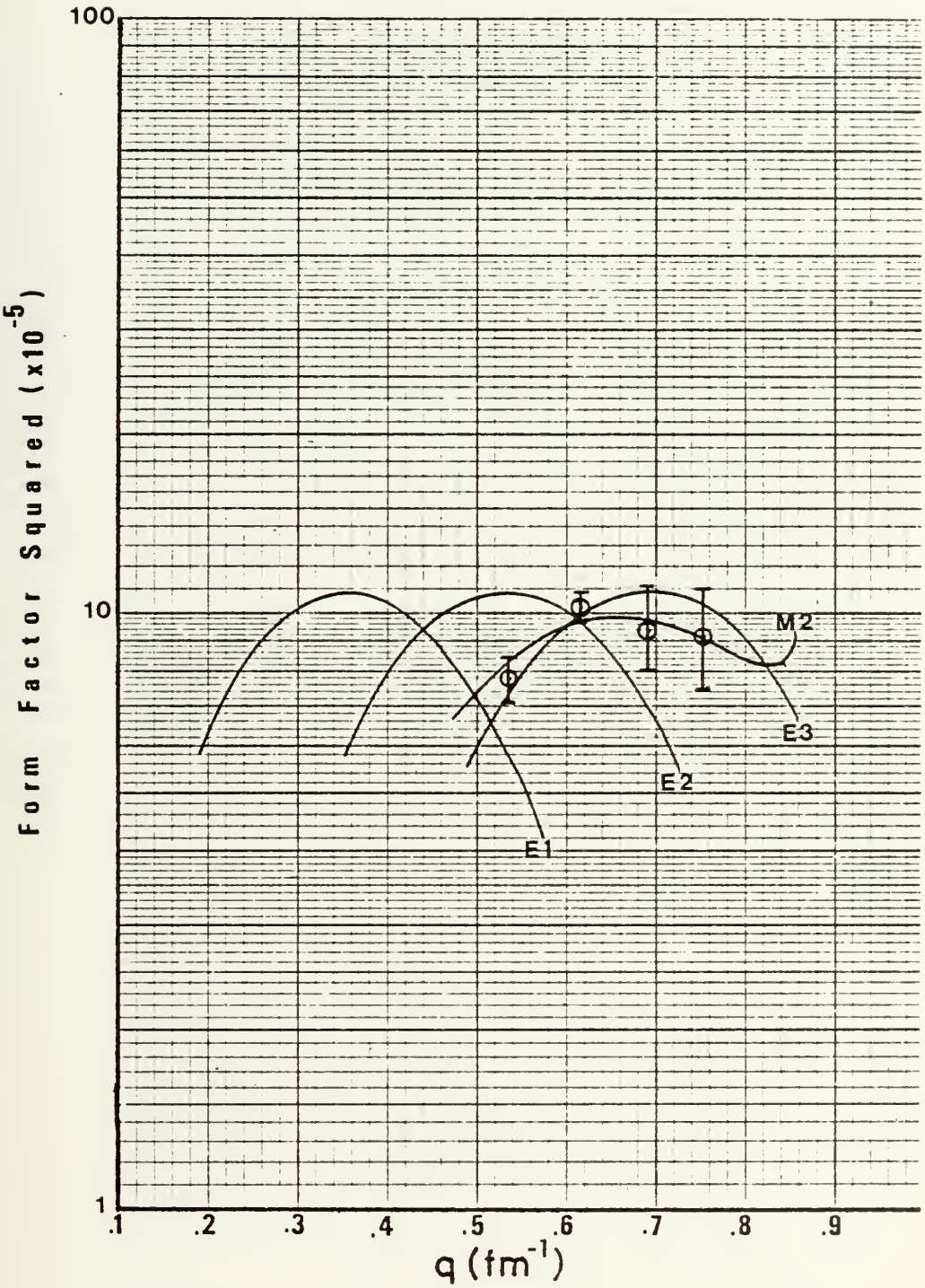

FIGURE 16. Experimental inelastic form factors for state at 13.63 MeV

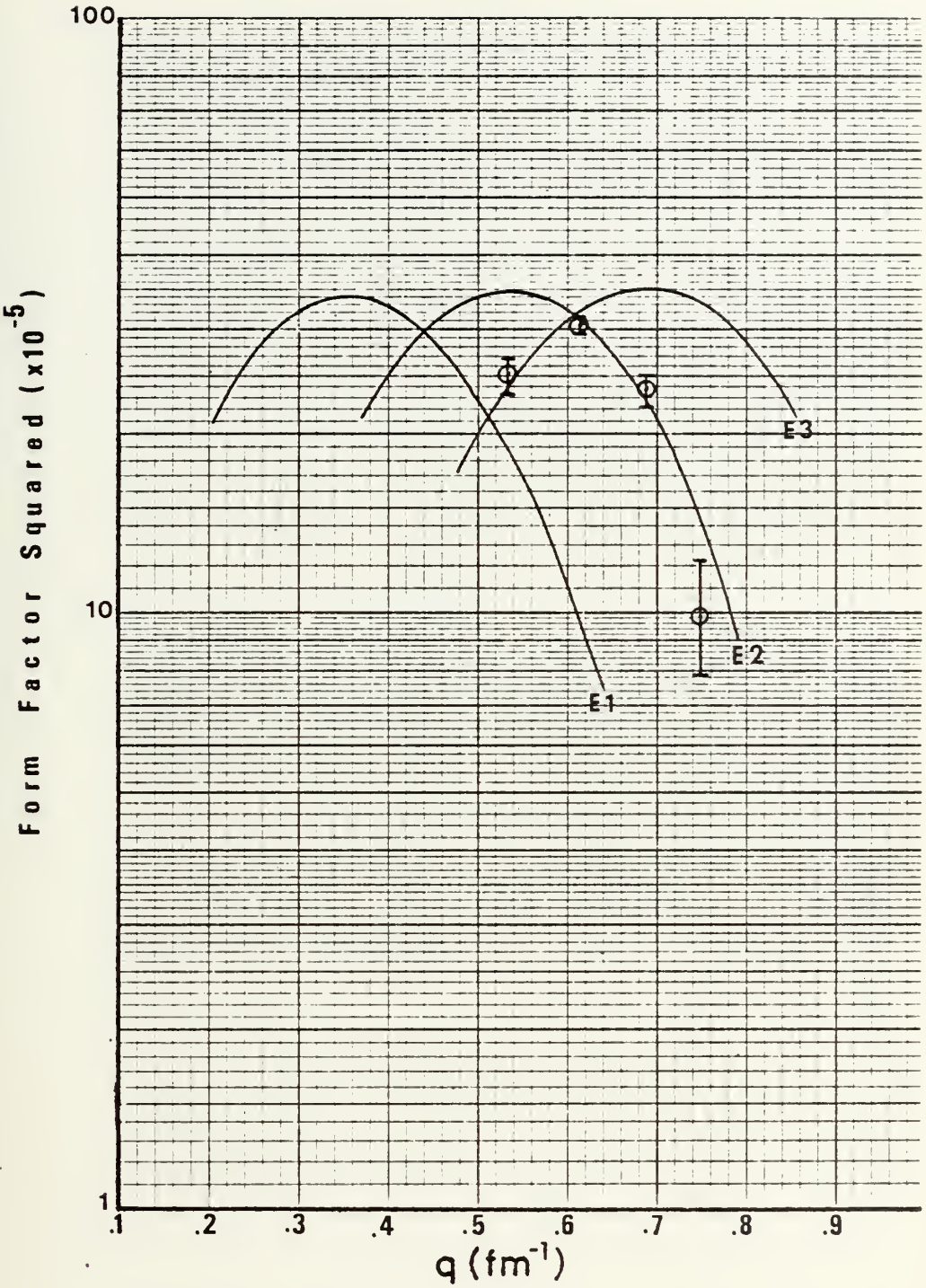

FIGURE 17. Experimental inelastic form factors for state at 14.86 MeV

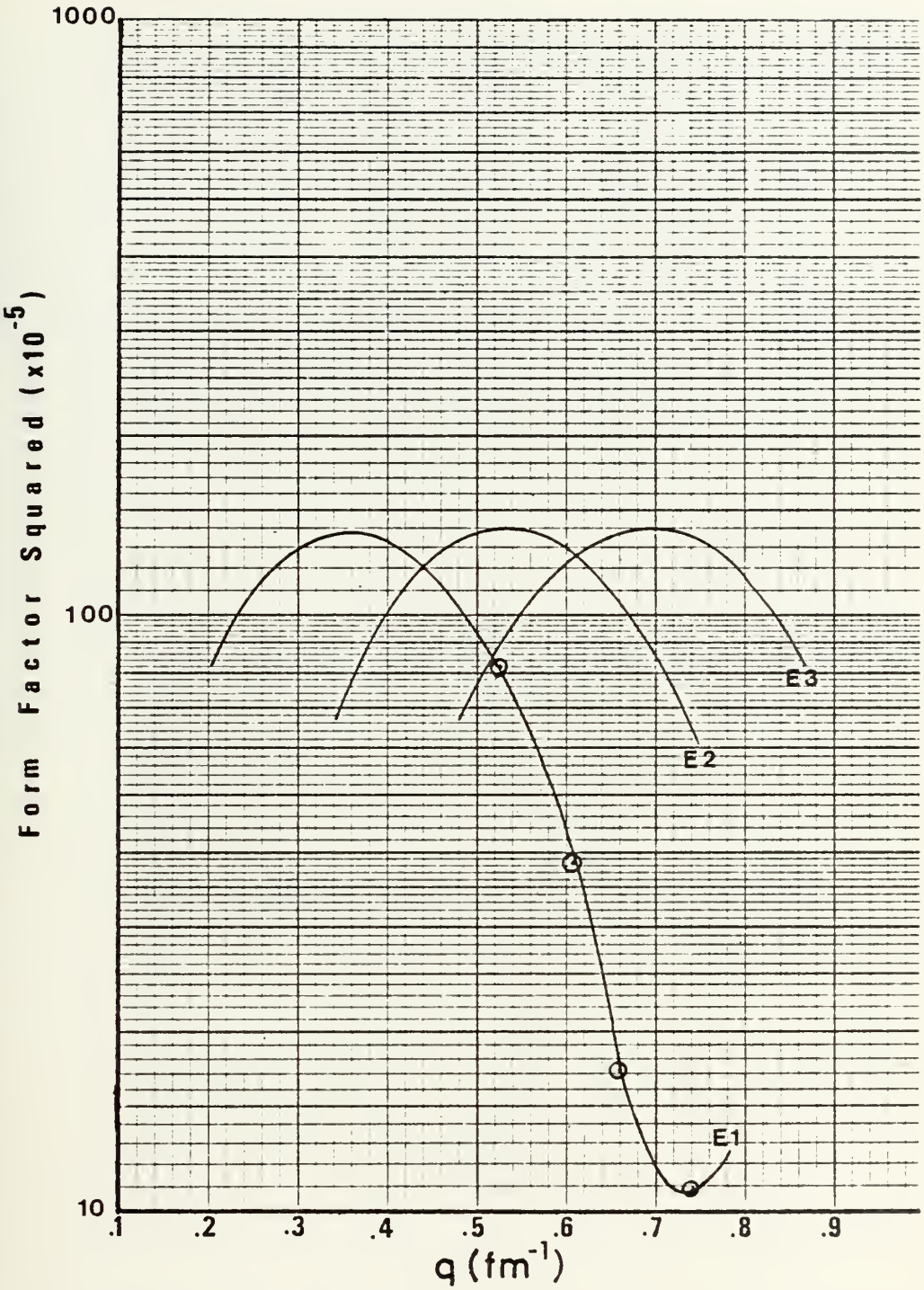

FIGURE 18. Experimental inelastic form factors for state at 16.60 MeV

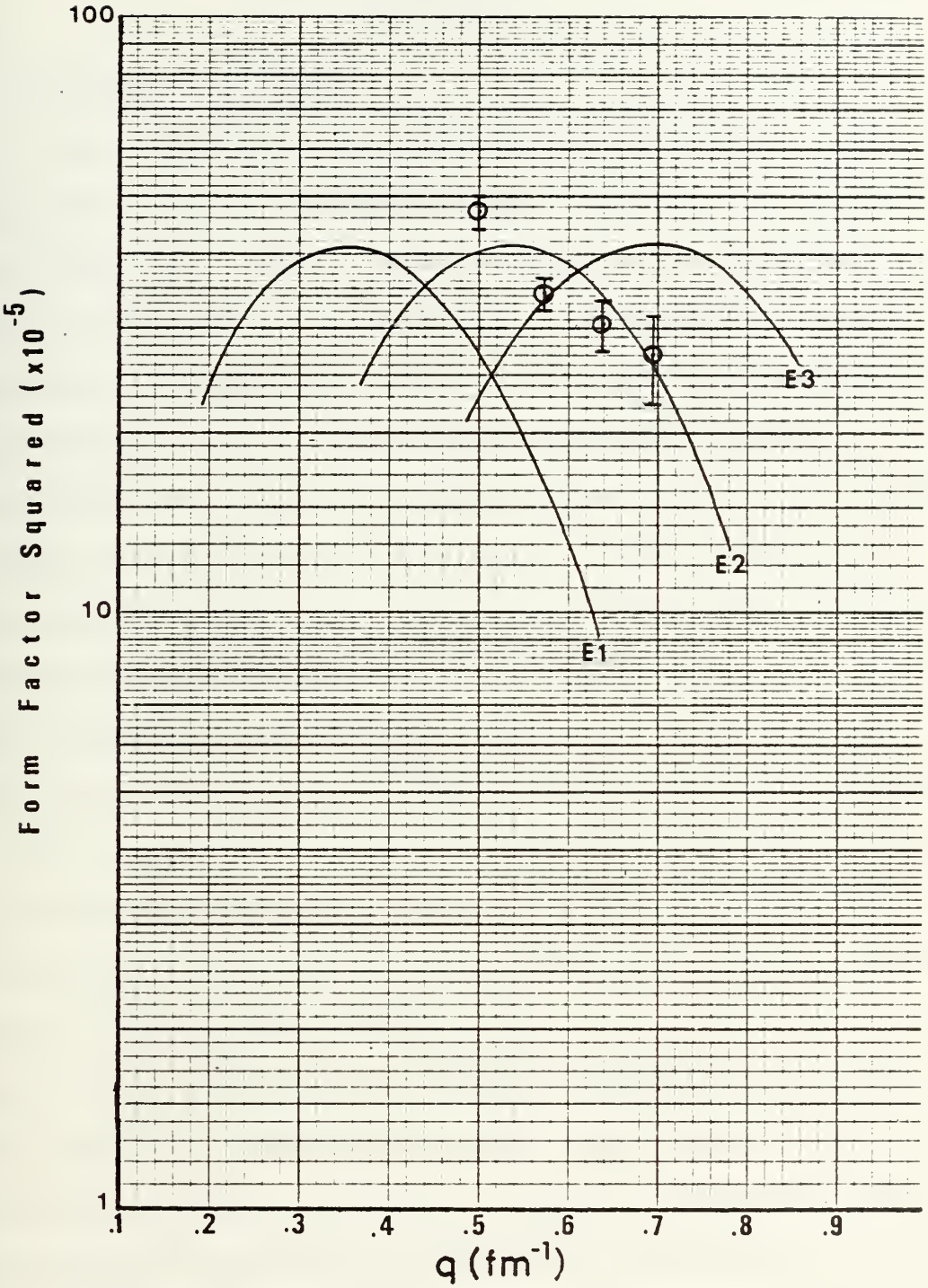

FIGURE 19. Experimental inelastic form factors for state at 27.85 MeV

IV. DISCUSSION

A. COLLECTIVE RESULTS

A total of nine transitions were determined to give consistent fits to the spectra at 75°, 90°, 105° and 120° (See Table VI). The χ^2 error per degree of freedom ranged from 0.86 at 105° to 1.08 at 75°. Observed variations in excitation energy and widths for the nine resonances were approximately 200 keV from their numerical averages. With few exceptions, the form factor values extracted from the fitting program compared favorably to DWBA calculations for the selected resonances. Some inconsistencies were noted in the extracted form factors for the 120° data. The relatively high background and possible transverse contributions to the cross section were contributing factors to these inconsistencies.

The iterative process of fitting the spectra was started by fixing the excitation energy, width and ratio of elastic to inelastic peak height for the E1 giant dipole resonance [Refs. (28) and (29)] at E_x = 16.6, Γ = 4.0 MeV and a peak height which resulted in a reduced transition strength of $B(E1)=19.7\ e^2 fm^2$. Once this was done the remaining data were fitted by visually determining possible resonance excitation energies and widths and allowing the fit program to search for appropriate heights. Throughout the early stages of data analysis, repeated attempts were made to fit the previously reported E2 giant quadrupole resonance with

$E_x \simeq 13.8$ and $\Gamma \simeq 3.2$ [Ref. (25)] to the data. Although values of $\chi^2 < 1.1$ were obtained in these attempts, the data showed a very distinct structure at $E_x = 13.6$ MeV which could not be satisfactorily fitted in conjunction with the reported E2 values. The inclusion of the resonance at $E_x = 13.6$ MeV with $\Gamma = 1.2$ MeV resulted in movement of the giant E2 resonance to $E_x = 14.8$ and $\Gamma = 3.0$ to correctly fit the data. The 90°, 105° and 120° spectra strongly supported the necessity for such a resonance and although its presence was less apparent in the 75° data, the resultant fit showed its existence. Once the fitting program was completed in the primary data sets, the resultant excitations were applied to the two alternate 90° data sets and the one extra 120° data set. Excellent ($\chi^2 < 1.0$) results were immediately obtained.

B. EXCITATIONS AND CHARACTERISTICS

1. 6.69 MeV

This state is a very well defined narrow line of $\Gamma = 0.97$ MeV which was given the assignment of an E2 bound state. Its width was twice the resolution width. The line structure was quite smooth in the 75°, 90°, and 105° data but became more erratic in the 120° data. The latter behavior can be explained by the low count rate and high background and the increasing transverse contributions to the scattering cross section at the backward angle. Using this reduced transition strength, the resonance accounts

for 7.7 ± 1.6% of the EWSR and 2.5 Weisskopf units for the E2 assignment. Visual inspection of form factor plot, Figure 11, favors the E2 assignment.

2. 8.09 MeV

This resonance is the second well defined line in the bound state region. The state has a width of Γ = 1.22 MeV and was also given an E2 assignment. Again the line structure in the data was quite smooth and easy to fit at 75°, 90°, and 105°. The assignment was made based on these angles and the resultant B(E2) value accounts for 11.0 ± 2.2% of ESWR and 2.9 Weisskopf units.

3. 10.01 MeV

The assignment of E2 at $45A^{-1/3}$ was based on 75°, 105° and 120° data. Considerable difficulty was encountered in attempting to fit the energy range from 10 MeV to 12 MeV due to the relatively slow count rate in comparison to the twin peaks at 6.69 MeV and 8.09 MeV and the giant resonance region. The resonance at 10.01 MeV was consistently erratic in all three 90° spectra since the number of counts was very low at that energy. The assignment of E2 accounts for 4.3 ± 0.4% of the EWSR and 0.9 Weisskopf units.

4. 11.21 MeV

The analysis of the state at $50A^{-1/3}$ MeV favored an E2 assignment. Since the DWBA form factors for E0 and E2 are very similar in the momentum transfer region of this study, both assignments were considered. The E2 assignment accounts for 3.7 ± 1.1% of the EWSR and has a strength corresponding

to 0.7 Weisskopf units. However, an E0 assignment exhausts 5.8% of the available monopole strength in Yttrium.

5. 12.46 MeV

The multipolarity assignment of the resonance at $56A^{-1/3}$ remains ambiguous. The extracted form factor values agreed most closely with an M2 assignment although an E3 assignment served almost as well. The M2 assignment displayed a strength of 17.5 Weisskopf units. An assignment of E3 exhausted 3.5 ± 0.7% of the EWSR and yielded a strength of 1.6 Weisskopf units.

6. 13.63 MeV

The existence of this resonance (at $61A^{-1/3}$) was strongly supported by all of the data. It was given an assignment of M2. The relatively narrow structure appeared in each spectrum, including the three separate 90° runs and the two separate 120° runs. Its presence was less obvious in the 75° spectrum but inclusion of the resonance improved the fit. The E2 giant resonance in ^{89}Y has been reported at 13.8 ± .2 MeV with a width of 3.2 from (p,p') work [Ref. (25)]. Electron scattering experiments in ^{90}Zr have reported the E2 GDR at E_x = 14.0 MeV and Γ = 4.8 MeV [Ref. (4)]. Therefore, the assignment of the relatively narrow line at this energy proceeded cautiously.

The extracted form factors compared favorably to both a M2 and an E3 assignment. An E3 assignment would have exhausted 7.7 ± 1.5% of the EWSR with a strength of 3.2 Weisskopf units. The M2 assignment had a reduced transition

strength correlating to 35.4 Weisskopf units. The electron scattering experiments should have shown the contribution of such a strong E3 mode if it were indeed present. However, in the latter experiment, an M2 resonance would have been obscured by the E2 because M2 and E2 display a similar dependence on q at very forward angles where the transverse character of a magnetic transition does not matter very much.

7. 14.86 MeV

The assignment of an E2 giant resonance at $66A^{-1/3}$ compares to some extent with the (p,p') experiments in ^{89}Y reported in Ref. [(25)] and with the (e,e') experiments in ^{90}Zr reported in Ref. [(4)]. The shift in excitation energy is a direct result of fitting the required resonance at 13.63 MeV. The data readily support the $66A^{-1/3}$ energy position and width of 3.0 MeV. Extracted form factors compared well with DWBA calculations for an E2 resonance and the assignment exhausts 24.6 ± 4.9% of the EWSR with a strength of 3.6 Weisskopf units. This relatively low exhaustion of EWSR compared very well with the results of the (p,p') experiments but was less than half the corresponding value reported for the (e,e') and the (α,α') experiments in ^{90}Zr. The latter observation prompted extensive attempts to fit the data with an E2 cross section that would account for about 50% exhaustion. The surprising result was that 90°, 105° and 120° data would support such a cross section with E_x = 14.0 MeV and Γ = 4.8 MeV and an exhaustion of 53% E2 EWSR. However, the 75° data, which

displayed a much smoother character in this area, would not accept such a large cross section. The largest E2 cross section able to fit the 75° data exhausted 35% EWSR and resulted in a poor fit ($\chi^2 = 1.4$). Repeated attempts to match the E2 cross sections through the four angles led irrevocably to the results reported in this paper. For a comparison of these different fitting attempts see Figures 6 and 20. It was also noted that (α,α') experiments reported in Ref. [(24)] describe the E2 giant resonance at $E_x = 14.5$ MeV, $\Gamma = 4.0$ MeV with an E2 EWSR exhaustion of 54%. Again no resonance of this description could be coaxed to properly fit all the available spectra.

8. 16.6 MeV

The resonance at $74A^{-1/3}$ is the known E1 giant dipole resonance reported from photonuclear work [Refs. (28) and (29)] and compares well with the reported position, width and strength of the E1 GDR in ^{90}Zr electron scattering experiment [Ref. (4)]. Considering the paucity of experimental data in ^{89}Y, this resonance was used exclusively as a known, fixed feature for the data fitting process. The results obtained on all other fitted resonances are therefore greatly dependent upon the correct assignment of $E_x = 16.6$, $\Gamma = 4.1$ and reduced transition strength of 19.7 (e^2MeV fm^2). These values were observed to fit the data very well and resulted in exhausting 100.6% of the EWSR with a strength of 5.1 Weisskopf units. The excellent results obtained from fixing this resonance lent confidence to the assignments of the remaining resonances.

Some evidence exists in the 75° data for the excitation of the $T_>$ [Ref. (34)] part of the E1 giant resonance at E_x = 20.3 MeV, but attempts to fit $T_>$ were unsatisfactory and the remaining angles offered no support for this resonance.

9. 27.92 MeV

The resonance at $125A^{-1/3}$ was given an E2 assignment and compares well with the predicted E2 isovector resonance of $135A^{-1/3}$ [Ref. (18)]. This assignment exhausted 46.3 ± 13.9% of the isovector E2 EWSR and the transition strength accounted for 4.6 Weisskopf units.

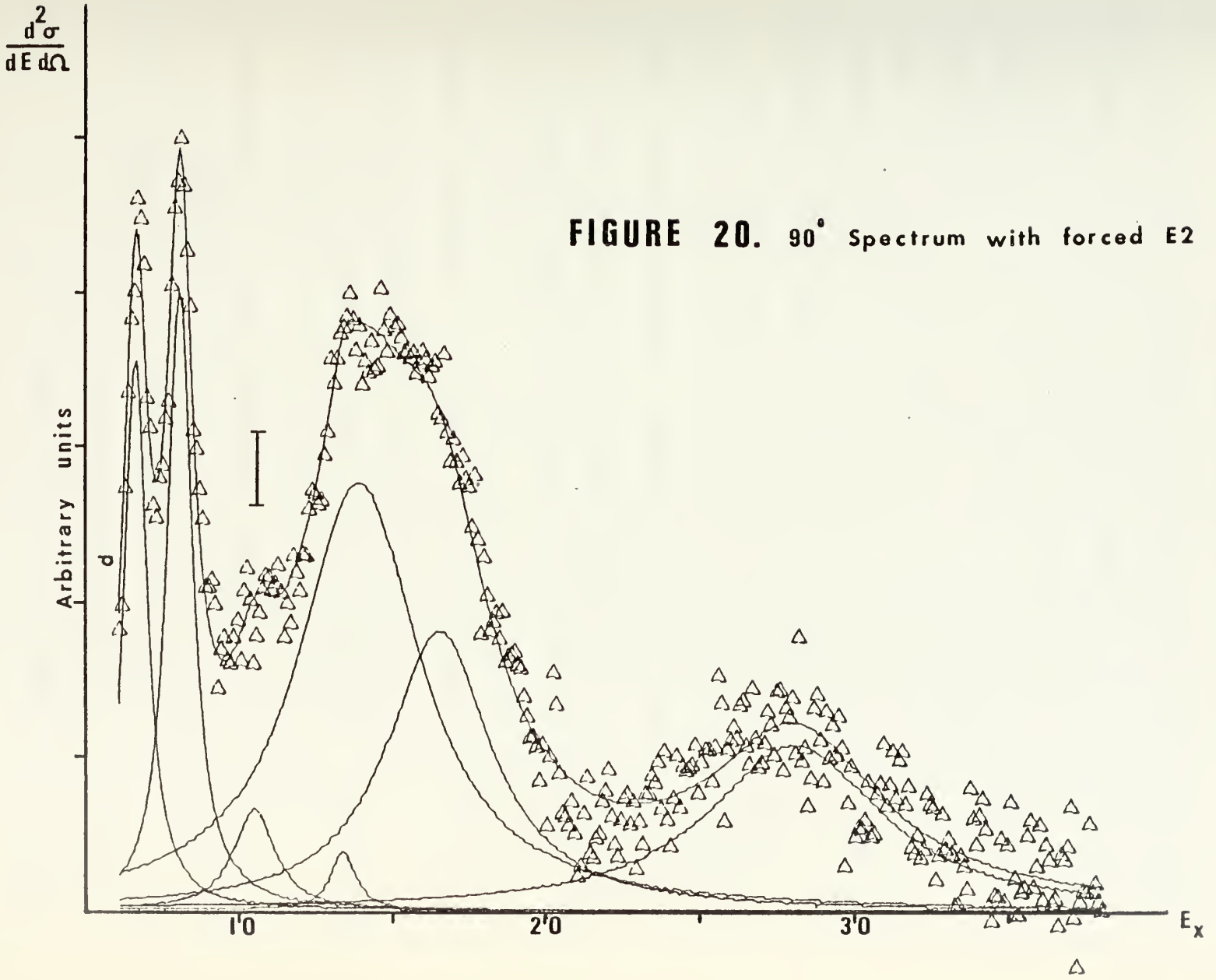

FIGURE 20. 90° Spectrum with forced E2

V. CONCLUSIONS

The spectrum of inelastically scattered electrons from ^{89}Y was studied in an excitation energy range from 6.1 MeV to 38.0 MeV. Five previously unreported states were observed below the (γ,η) threshold. Four giant resonances were observed at 13.63, 14.86, 16.6 and 27.92 MeV. Of these, the 13.63 MeV M2 and the 27.9 MeV E2 isovector resonances have not been previously reported. Multipolarity assignments were made as discussed in Section IV.B.

The 16.6 MeV resonance was identified as the widely studied E1 giant dipole resonance and was used as a starting value for data analysis. Although the assignments of the M2 at 13.63 MeV and the E2 giant quadrupole at 14.8 MeV do not support existing studies in this and neighboring elements [Refs. (25), (4) and (24)], the assignments were considered positive. Previous (e,e') studies of a N = 50 nucleus were conducted at forward scattering angles [Ref. (4)] and therefore would not be expected to distinguish the M2 from the E2 cross section. Transverse magnetic contributions may also have been present in the 6.69 and 8.09 MeV states at 120°. Further study in the backward angles should be made with better statistics.

The E2 resonance at 27.92 MeV was observed as predicted in Ref. [(18)] and is believed to be the isovector E2 giant resonance.

LIST OF REFERENCES

1. Pitthan, R. and others, Phys. Rev. Ltrs. 33, 849(1974).

2. Moore, G.L. and others, Widths of the E2 ($\Delta T=0$ and $\Delta T=1$) Giant Resonances in ^{165}Ho, paper to be published in Z. Naturforschung, Part a.

3. Pitthan, R. and Walcher, T., Phys. Rev. Ltrs, 368, 563(1971).

4. Fukuda, S. and Torizuka, Y., Phys. Rev. Ltrs, 29, 1109(1972).

5. Rutherford, E., Phil. Mag. 21, 669(1911).

6. Mott, N.F., Proc. Roy. Soc. Ser. A 124, 426(1926).

7. Uberall, H., Electron Scattering from Complex Nuclei, Academic Press, New York (1971).

8. Hofstadter, R., Rev. Mod. Phy. 28, 214(1956).

9. Theissen, H., Spectroscopy of Light Nuclei by Low Energy (<70 MeV) Inelastic Electron Scattering, Institut fur Technische Kernphysik der Technischen Hochschule, Darmstadt (1972).

10. Ziegler, F.F. and Peterson, G.A., Phys. Rev. 165, 1337(1968).

11. Yennie, D.R., Ravenhall, D.G. and Wilson, R.N., Phys. Rev. 95, 500(1954).

12. Rawitscher, G.H. and Fischer, C.R., Phys. Rev. 122, 1330(1961).

13. Ziegler, J.F., The Calculation of Inelastic Electron Scattering by Nuclei (1967): Available from the Clearing House for Federal Scientific and Technical Information, National Bureau of Standards, U.S. Department of Commerce, Springfield, Va. 22151, under Publication Number Yale 2726E-49.

14. Tassie, L.J., Austr. J. Phys. 9, 407(1956).

15. Isabelle, D.B. and Bishop, G.R., Nuc. Phys. 45, 209(1963).

16. Berman, B.L. and Fultz, S.C., Rev. Mod. Phys. 47 3, 713(1975).

17. Pitthan, R. and Walcher, T., Z. Naturforsch. 27a, 1683(1972).

18. Bohr, A. and Mottelson, B., Nuclear Structure Vol. II, W.A. Benjamin, Inc., London, 1975.

19. Buskirk, F.R., Giant Resonances in Heavy Nuclei Measured by Inelastic Electron Scattering, paper presented to the Annual Meeting of the America Physical Society, Anaheim, Cal., January 1975.

20. Shafroth, S.M., Trehan, P.N. and Van Patter, D.M., Phys. Rev. 129, 704(1963).

21. Stautberg, M.M., Kraushaar, J.J. and Ridley, B.W., Phys. Rev. 157, 977(1967).

22. Peterson, G.A. and Alster, J., Phys. Rev. 166, 1136(1968).

23. Hasinoff, M., Fisher, G.A. and Hanna, S.S., Nuc. Phys. A216, 221(1973).

24. Youngblood, D.H. and others, Phys. Rev. C13(3), 994(1976).

25. Bertrand, F.E., Excitation of Giant Multipole Resonances Through Inelastic Scattering, to be later published in Annual Review of Nuclear Science, Oak Ridge, Tennessee, 1976.

26. Alster, J., Shreve, D.C. and Peterson, R.J., Phys. Rev. 144, 999(1966).

27. Hinricksen, P.F., Shafroth, S.M. and Van Patter, D.M., Phys. Rev. 172, 1134(1968).

28. Berman, B.L. and others, Phys. Rev. 162, 1098(1967).

29. Leprêtre, A. and others, Nuc. Phys. A175, 609(1971).

30. Barnett, M.T. and Cuneen, W.J., Design and Performance of the Electron Linear Accelerator at the U.S. Naval Postgraduate School, Master's Thesis, U.S. Naval Postgraduate School, Monterey, 1966.

31. Warshawsky, A.S. and Webber, A.M., Giant Multipole Resonances in ^{197}Au, Master's Thesis, U.S. Naval Post-Graduate School, Monterey, 1973.

32. Gordon, E.F., An Investigation of the Natural Line Shape of the Giant Dipole Resonance, Master's Thesis, U.S. Naval Postgraduate School, Monterey, 1975.

33. Moore, G.L., Electroexcitation of Giant Resonances Between 5 MeV and 30 MeV Excitation Energy in ^{165}Ho, Master's Thesis, U.S. Naval Postgraduate School, Monterey, 1974.

34. Fallieros, S., Goulard, B., and Venter, R.H., Phys. Ltrs. 19(5), 398(1965).

35. Atlas of Photonuclear Cross Sections Obtained with Monoenergetic Photons, Second Edition, Lawrence Livermore Laboratory, 1974.

36. Bohr, A. and Mottelson, B., Some Current Themes in Nuclear Research, Papers communicated privately to Pitthan, R. and Buskirk, F.R., 1974.

37. Comfort, J.R., and others, Phys. Rev. C11(6), 2012(1975).

38. Ferlic, K.P. and Waddell, R.D., Electroexcitation of Giant Resonances Between 5 MeV and 40 MeV Excitation Energy in ^{197}Au, Master's Thesis, U.S. Naval Postgraduate School, Monterey, 1974.

39. Fivozinsky, S.P. and others, Phys. Rev. C 9(4), 1533(1974).

40. Hulstman, L., and others, Nuc. Phys. A251, 269(1975).

41. Oak Ridge National Laboratory Report ORNL-TM-4347, New Giant Resonances in Nuclei, by G.R. Satchler, September 1973.

42. Ramavataram, K. and others, Nuc. Phys. A247, 139(1975).

43. Torizuka, Y. and others, Giant Resonances Other Than E1, Paper presented at the International Conference on Photonuclear Reactions and Applications, Pacific Grove, California, 26-30 March 1973.

44. Walcher, T., Giant Resonances, Paper presented at the Institut fur Kernphysik, Darmstadt, Germany, 1973.

45. Ziegler, J.F. and Peterson, G.A., Collective Excitations in Pb^{206}, Pb^{207}, Pb^{208} and Bi^{209} By Inelastic Electron Scattering, Ph.D. Thesis, Yale University, Hartford, 1967.

INITIAL DISTRIBUTION LIST

		No. Copies
1.	Defense Documentation Center Cameron Station Alexandria, Virginia 22314	2
2.	Library, Code 0212 Naval Postgraduate School Monterey, California 93940	2
3.	Physics Library, Code 61 Department of Physics and Chemistry Naval Postgraduate School Monterey, California 93940	2
4.	Professor F.R. Buskirk, Code 61Bs Department of Physics and Chemistry Naval Postgraduate School Monterey, California 93940	5
5.	Professor W.R. Pitthan, Code 61Pt Department of Physics and Chemistry Naval Postgraduate School Monterey, California 93940	5
6.	Professor J.N. Dyer, Code 61Ey Department of Physics and Chemistry Naval Postgraduate School Monterey, California 93940	1
7.	Associate Professor E.B. Dally, Code 61Dd Department of Physics and Chemistry Naval Postgraduate School Monterey, California 93940	1
8.	LCDR. James O. Shannon, USN USS GRIDLEY CG-21 c/o Fleet Post Office San Francisco, California 96601	2
9.	LT. William H. Smith, USN 8879 Aquarius Dr. San Diego, California 92126	1
10.	Dr. X.K. Maruyama National Bureau of Standards Center for Radiation Research Gaithersburg, Maryland 20760	1